Lipopolysaccharide stimulates dynamic changes in B cell metabolism to promote proliferation

Dana M.S. Cheung[1], Momchil Razsolkov[1], Fabrizia Bonacina[2], Stephen Andrews[1], Megan Sumoreeah[1], Linda V. Sinclair[1], Andrew J.M. Howden[1] and J. Simon C. Arthur[1*]

1) Division of Cell Signalling and Immunology, Faculty of Life Sciences, University of Dundee, Dow Street, Dundee, DD1

2) Department of Pharmacological and Biomolecular Sciences "Rodolfo Paoletti", University of Milan, via Balzaretti 9, 20133, Milan, Italy

*Corresponding Author. j.s.c.arthur@dundee.ac.uk, Division of Cell Signalling and Immunology, School of Life Sciences, University of Dundee, Dow St, Dundee, DD1

Keywords:

B cell/cholesterol/transporter/toll-like receptor/statin

Summary

Naïve B cells exit quiescence and enter a proliferative state upon activation, ultimately differentiating into antibody-secreting or memory B cells. Toll-like receptor (TLR) ligands, such as lipopolysaccharide (LPS), can serve as physiological stimuli to initiate this transition. Using quantitative proteomics, we show that TLR4 engagement induces metabolic reprogramming in murine B cells, increasing the expression of amino acid transporters and cholesterol biosynthetic enzymes. The amino acid transporter SLC7A5 is markedly upregulated following LPS stimulation, and conditional deletion of *Slc7a5* impairs B cell proliferation, underscoring its essential role in B cell activation. LPS also elevates intracellular cholesterol levels, and inhibition of the rate-limiting enzyme HMG-CoA reductase blocks proliferation. This effect was mediated by a dual requirement for cholesterol metabolism and protein prenylation downstream of HMG-CoA reductase. Notably, this was not unique to TLR4 signalling but is also observed in B cells activated via TLR7, TLR9, CD40, or the B cell receptor. Together, these findings reveal that metabolic rewiring, including amino acid uptake and cholesterol metabolism, is an essential feature of B cell activation and proliferation.

Introduction

B cell activation can be initiated through either T cell-dependent (TD) or T cell-independent (TI) pathways, with TI activation further subdivided into a type I or type II response depending on the stimuli. During TD activation, following recognition of a protein antigen via the B cell receptor (BCR), the B cell can present peptides from the antigen to CD4 T cells, resulting in T cell activation. Additionally, the B cell receives co-stimulation through the binding of its CD40 receptor to the CD40 ligand found on T cells, which promotes differentiation, proliferation, somatic hypermutation, and class switch recombination (CSR) (Hoffman *et al*, 2016). Type I TI responses are activated by agonists such as lipopolysaccharide (LPS), which bind to toll-like receptors (TLRs) on B cells to induce a strong proliferative signal and increase antibody production. Longer-term exposure to LPS can also promote the differentiation of plasma cells (Genestier *et al*, 2007). Conversely, type II TI antigens consist of long repetitive structures, such as polysaccharides, which at high concentrations crosslink multiple BCRs to stimulate proliferation and antibody production (Obukhanych & Nussenzweig, 2006).

A well-established model to study TI B cell activation is to use LPS, a component of the cell wall of gram-negative bacteria, which stimulates TLR4 (Hoshino *et al*, 1999; Poltorak *et al*, 1998) to induce robust B cell proliferation and antibody secretion, both *ex vivo* (Coutinho *et al*, 1974; Dziarski, 1982) and *in vivo* (Johnson *et al*, 1956). Upon activation, TLR4 propagates downstream signalling through the adaptor proteins MyD88 and TRIF. This in turn activates pathways, including MAPK and NF-κB signalling, to elicit the required physiological response (Arthur & Ley, 2013; Kawai *et al*, 2024). The essential role of TLR4 in LPS-induced activation of B cells has been demonstrated by studies using TLR4-deficient mice. B cells from TLR4 or Myd88 knockout mice did not proliferate in response to LPS or lipid A stimulation *ex vivo* (Hoshino *et al*, 1999; Kawai *et al*, 1999). Similarly, in studies where B cells from MyD88- and TLR4-knockout mice were transferred into μMT mice (that lack mature B cells), a significant reduction in IgG1 production was observed (Pasare & Medzhitov, 2005).

Naïve B cells have been shown to be in a quiescent state with low metabolic demand (Waters *et al*, 2018). Conversely, B cell activation must require a significant increase in biomolecules such as proteins, lipids, and nucleic acids to support their rapid expansion and proliferation. The existing literature has focused on the role of glucose and glucose transporters in B cell function. Previous studies have demonstrated that activation using LPS or anti-IgM to stimulate the BCR increases glucose uptake and leads to an increased oxygen consumption rate (Dufort *et al*, 2007; Jellusova *et al*, 2017). Whether this corresponds to changes in metabolic enzymes at a proteomic level, and whether TI B cell activation utilises other metabolic pathways, remains unknown. This increased glucose uptake has been shown to provide precursors for ribonucleotide and lipid synthesis (Waters *et al*, 2018). Similarly, the deletion of *Slc2a1* (which encodes for glucose transporter GLUT1) impaired germinal centre formation,

plasma cell differentiation, and the production of high-affinity antibodies (Bierling *et al*, 2024; Brookens *et al*, 2023). Recent reviews have expressed the need for studies investigating metabolic changes in activated B cells, especially the role of lipid metabolism, which is poorly understood (Johnstone *et al*, 2024; Peeters & Jellusova, 2023).

T cell activation has been shown to stimulate global changes in metabolism at a proteomic level (Procaccini *et al*, 2016; Howden *et al*, 2019; Tan *et al*, 2017). However, there are no comparable proteomic studies that demonstrate how B cells support the change in metabolic requirements and energy demand from quiescence to activation upon LPS stimulation. Therefore, we used Data Independent Acquisition (DIA) based mass spectrometry to profile the B cell response to a combination of LPS + Interleukin 4 (IL-4) stimulation, a well-established *ex vivo* model of TI B cell activation. From this, we identified a substantial upregulation of proteins involved in multiple metabolic pathways, including amino acid uptake and cholesterol biosynthesis. We demonstrate the requirement of L-amino acid transporter SLC7A5 for B cell survival and proliferation *ex vivo*. Similarly, we highlight the necessity of both cholesterol metabolism and protein prenylation downstream of the rate-limiting enzyme HMG-CoA reductase for B cell growth, survival, and proliferation. These results highlight the pronounced metabolic rewiring induced downstream of LPS + IL-4 stimulation.

Results

LPS + IL-4 stimulation of murine B cells promotes proliferation and changes the expression of enzymes involved in cellular metabolism

Previous studies have shown that *ex vivo* stimulation of murine B cells with LPS and IL-4 can drive B cell proliferation and class switching to IgG1 (Snapper *et al*, 1988). Consistent with this, we found that lymphocytes isolated from lymph nodes and subsequently stimulated with LPS + IL-4 resulted in the proliferation of CD19+ B cells, as judged by dilution of Cell Trace Violet (CTV) labelling. LPS + IL-4 stimulation led to extensive proliferation, with up to 6 generations of B cells present after 72 hours (Figure 1A). Proliferation itself is thought to be a prerequisite for cells to undergo class-switching (Hodgkin *et al*, 1996). In line with this, only LPS + IL-4 stimulated B cells found in later generations were positive for IgG1 (Figure 1A). On a similar note, cell size is considered a key regulator of the G1/S transition, as progression through the cell cycle can only continue once a certain threshold in size has been reached (Barberis *et al*, 2007). Accordingly, we found that 72 hours of LPS + IL-4 stimulation led to a marked increase in cell size and granularity as indicated by a higher forward/side scatter compared to naïve B cells (Figure 1B-D). Stimulation with IL-4 alone resulted in a smaller increase in cell size than a combination of LPS + IL-4, but did not give rise to a strong proliferative response or class switching (Figure 1A-D). Naïve B cells were used for comparison in ongoing experiments, as surviving unstimulated B cells exhibited a similar phenotype in the flow cytometry analysis;

however, the lack of stimulation led to significant cell death from 24 hours onwards (Figure S1A-B).

These functional differences following activation suggest a significant change may be occurring at the protein level. To investigate this further, we analysed changes in the proteome after 24 hours of stimulation, as this time point was sufficient for B cells to increase in size but retain their synchrony in terms of the number of divisions they had undergone *ex vivo*. DIA-based mass spectrometry was used to compare the proteomes of naive B cells to activated B cells after 24 hours of LPS + IL-4 stimulation. The proteomic ruler method (Wiśniewski *et al*, 2014) was then used to estimate protein copy numbers and concentration. Using this approach, a total of 8030 protein species were identified, of which 7187 were quantified in both naïve and LPS + IL-4 stimulated B cells. Based on the mass spectrometry data, the predicted total protein mass in the B cells increased by approximately 2-fold following stimulation with a combination of LPS + IL-4 (Figure 1E). This change in protein mass was due to an increased copy number of most proteins in the cell (Figure 1F), with a median $\log_2$ fold increase of 1.04. To adjust for the increase in cell size, the fold change in protein concentration was analysed, as this provides an indication of what proteins are selectively upregulated or downregulated as opposed to those that scale with cell size.

For the data using estimated cellular concentrations, using cutoffs of $q < 0.05$ and a log2 fold change more than one standard deviation away from the median, 863 proteins were found to be upregulated following activation, while a further 301 were detected in all of the stimulated B cells but none of the naïve ones. 409 proteins were downregulated in the LPS + IL-4 stimulated B cells in comparison to naïve B cells, while a further 57 were detected in the naïve B cells, but none of the activated B cells (Figure 1G).

To identify the biological pathways that were affected by LPS + IL-4 stimulation, proteins that were classified as regulated using the criteria above were searched against Gene Ontology (GO) Biological Processes terms and *Kyoto Encyclopaedia of Genes and Genomes* (KEGG) databases. Enrichment analysis on the downregulated proteins did not highlight any specific processes. However, upregulated proteins were associated with terms related to the cell cycle, ribosome biogenesis, protein translation, and steroid biosynthesis (Figure 1H, Table S1).

While changes in the above processes would make sense in terms of cell proliferation, it was notable that changes in the glycolytic and oxidative phosphorylation pathways were not highlighted in this analysis. Previous studies have indicated that there is an increased demand for glucose in LPS-activated B cells (Dufort *et al*, 2007; Johnstone *et al*, 2024). Isotope tracing experiments following CD40L and IL-4 activation to stimulate proliferation have suggested that this increased glucose uptake is used in the pentose phosphate pathway, potentially to provide NADPH and precursors for nucleotide biosynthesis, while alternative carbon sources may be used to drive an increase in the TCA cycle and oxidative phosphorylation (Waters *et al*, 2018). The levels of enzymes involved in glucose metabolism were therefore examined in the

proteomic data. In general, changes in the estimated concentrations of proteins involved in glycolysis, pentose phosphate pathway, TCA cycle, or oxidative phosphorylation were not observed (Figure S2A, B), although their copy numbers did increase in proportion to the increase in cell size (Figure S2C, D). B cells express the SLC2A1 (Glut1) glucose transporter, and deletion of this gene has been shown to reduce B cell activation *in vivo* (Bierling *et al*, 2024; Brookens *et al*, 2023). There was an increase in the concentration of SLC2A1, which would be consistent with an elevated ability to take up glucose (Figure S2E). In addition, there was a 13-fold increase in hexokinase 2 (HK2), one of the enzymes involved in catalysing the 1st committed step for glucose to enter the glycolytic or pentose phosphate pathways (Tanner *et al*, 2018) (Figure S2F) and has recently been shown to be required for maximal B cell responses to *ex vivo* stimulation with LPS (Paradoski *et al*, 2024). To investigate if the increased copy number of Electron Transport Chain proteins correlated with changes in mitochondrial volume, B cells were stained with MitoTracker Red, a fluorescent dye that binds to mitochondria. We found that MitoTracker staining was significantly increased following 24 hours of LPS + IL-4 stimulation (Figure S2G, H).

Notably, one of the enriched processes was identified as the 'response to interferon alpha'. To take this further, we compared our data with a previously published RNAseq dataset that looked at the effect of IFNα on murine B cells (Mostafavi *et al*, 2016). We found that the majority of the IFNα regulated genes were not significantly upregulated at a protein level following LPS + IL-4 stimulation compared to naïve B cells (Figure S3A). IFNα and IFNβ signalling requires phosphorylation of the transcription factor STAT1 to induce transcription of type I IFN-dependent genes (Platanias, 2005). We found that LPS stimulation did not lead to detectable phosphorylation of STAT1 compared to stimulation with IFNβ (Figure S3B-C). Together, this suggests that there is not a strong interferon response in this system. It is possible, however, that as we stimulated lymph node cells before sorting for B cells for the proteomic experiment, a low level of type I interferon production from myeloid cells may have occurred, which could have contributed to a weak IFN gene signature in the B cells.

LPS + IL-4 stimulation upregulates proteins involved in the cell cycle

Stimulation with LPS + IL-4 causes B cells to exit from a quiescent state and start to proliferate (Figure 1). This was confirmed using DAPI staining, which demonstrated that while naïve B cells were predominantly in a G0/1 state, after 24 hours of LPS + IL-4 stimulation, the proportion of B cells in the S and G2 stages of the cell cycle were increased (Figure 2A, B). Progression through G1 is associated with an increase in Cyclin D expression, and activation of CDK4 and 6 (Rubin *et al*, 2020). At the same time, inhibitory cell cycle proteins such as p27Kip1 (Cdkn1b) are downregulated (Wagner *et al*, 1998). Therefore, we analysed the proteomic data for evidence of these changes. In naïve B cells, Cyclin D was not detected, while levels of CDK4 and 6 were low (Figure 2C-E). The levels of Cyclin D, CDK4, and CDK6 were all increased

202 following stimulation (Figure 2C-E). Naïve B cells also expressed high levels of
203 p27Kip1, and this was reduced by LPS + IL-4 stimulation (Figure 2F).

204 During the cell cycle, unphosphorylated RB1 binds to the E2F1/2/3 transcription factor,
205 preventing the transcription of genes required for cell cycle progression. Increased
206 CDK4/6 activity initiates RB1 phosphorylation, reducing its interaction with E2F, and
207 resulting in the induction of E2F target genes, allowing progression through G1 to the
208 S phase of the cell cycle (Engeland, 2022; Rubin *et al*, 2020). Increased
209 phosphorylation of RB1 was observed in B cells following LPS + IL-4 stimulation
210 (Figure 2G, H). In line with the increased RB1 phosphorylation, the levels of protein
211 expressed from known E2F target genes, such as *Mcm2-7, Pcna, Dhfr, Rrm1/2,* and
212 *Pola*3 (Chicas *et al*, 2010; Engeland, 2022; Leone *et al*, 1998; Wagner *et al*, 1998)
213 were increased following LPS + IL-4 stimulation (Figure 2I). Further progression
214 through the cell cycle requires Cyclins E, A, and B, as well as CDK2 and CDK1. While
215 Cyclin E was not detected in the proteomic data, the levels of Cyclin A, Cyclin B, CDK2,
216 and CDK1 were all increased by LPS + IL-4 stimulation (Figure 2J-M).

217

218 Protein synthesis in LPS + IL-4 stimulated B cells is dependent on the 219 uptake of amino acids

220 The cell growth and proliferation promoted by LPS + IL-4 stimulation would be
221 expected to require an increased rate of protein synthesis. This is consistent with the
222 proteomic analysis, which demonstrated an increase in total protein content within
223 activated B cells (Figure 1E) and an enrichment of proteins associated with protein
224 translation, including proteins that regulate ribosome biogenesis and the ribosomes
225 themselves (Figure 1H). The ribosome is composed of 40S and 60S subunits, each
226 of which is composed of multiple proteins (Doudna & Rath, 2002). LPS + IL-4
227 stimulation increased the total concentration of ribosomal proteins that make up both
228 the 40S and 60S subunits (Figure 3A, B). This overall increase was due to higher
229 expression of most of the individual proteins that make up the subunits, rather than a
230 large increase in one or two of the proteins (Figure 3C, D). In line with the increase
231 in ribosomal proteins, there was also an upregulation of proteins associated with
232 ribosome biogenesis (Figure 3E-G). To determine if this correlated with an increased
233 rate of protein synthesis, we measured the incorporation of the puromycin analogue
234 o-propargyl-puromycin (OPP) into newly synthesised proteins. Consistent with the
235 upregulation of ribosomal proteins, OPP incorporation was significantly higher in B
236 cells stimulated with LPS + IL-4 for 24 hours compared to naive B cells (Figure 3H-I).
237 Since LPS + IL-4 stimulation increased OPP incorporation, we tested whether this
238 was a stimulus-specific effect or whether other stimuli known to activate B cell
239 proliferation could increase protein synthesis. Murine B cells also respond to
240 agonists of TLR7 (Weeratna *et al*, 2005) and TLR9 (Arunkumar *et al*, 2013; Yi *et al*,
241 1998). Both the TLR7 agonist Resiquimod and the TLR9 agonist CpG increased
242 OPP incorporation in B cells (Figure S4A-B). Naive B cells can also be activated *ex*
243 *vivo* by ligation of their BCR with anti-IgM antibodies or by stimulation with CD40

244 ligand (CD40L). Similar to TLR agonists, both stimuli also increased OPP
245 incorporation in B cells (Figure S4A-B).

246 Elevated protein synthesis during rapid proliferation would require an increased supply
247 of amino acids. B cells have also been reported to increase amino acid biosynthesis
248 upon stimulation. scRNAseq has shown that cycling B cells express higher levels of
249 mRNA for enzymes in the serine biosynthetic pathway (D'Avola *et al*, 2022).
250 Furthermore, the level of these proteins, as well as rates of serine biosynthesis, were
251 found to be increased by stimuli such as anti-IgM, CD40L, and CpG, which are known
252 to induce B cell proliferation (D'Avola *et al*, 2022). While this was not further addressed
253 in the current study, the proteomic data reported here did show that serine biosynthetic
254 enzymes, including the rate-limiting enzyme PHDGH, were increased in response to
255 LPS + IL-4 stimulation (Figure S5).

256 Increased synthesis alone cannot satisfy the increased need for amino acids in
257 proliferating cells, as the cell is unable to make essential amino acids. Several
258 plasma membrane amino acid transporters were detected in the proteomic analysis,
259 and these were all found to be upregulated in response to stimulation with LPS + IL-
260 4 (Figure 4A). To look at the requirement for increased amino acid uptake during B
261 cell proliferation more closely, we focused on Lat1, a member of the System L
262 transporters. Lat1 is a heterodimer composed of an amino acid transporting light
263 chain subunit, SLC7A5, and a chaperone heavy chain subunit, SLC3A2 (CD98)
264 (Napolitano *et al*, 2015). Both of these subunits were upregulated in the proteomic
265 data following LPS + IL-4 stimulation (Figure 4B, C). Additionally, the upregulation of
266 SLC3A2 was confirmed by flow cytometry (Figure 4D, E). To determine whether this
267 increased protein expression resulted from increased transcription of the relevant
268 genes, we analysed RNA-Seq data generated from short-term LPS stimulation of
269 murine B cells (Tesi et al, 2019). Both SLC7A5 and SLC3A2 mRNA expression was
270 significantly upregulated following LPS stimulation (Figure S6A-B). A similar study
271 using anti-IgM and anti-CD40 to activate murine B cells has found an upregulation of
272 amino acid transporters, including SLC7A5, in their proteomic data, suggesting that
273 this is not a stimulus-specific effect (James *et al*, 2024).

274 *Slc7a5*$^{fl/fl}$/Vav-iCre^{+ve} mice, which have a deletion of SLC7A5 in all hematopoietic cells,
275 have a comparable number of naive B cells to wild-type (WT) controls, indicating that
276 SLC7A5 is not critical for initial B cell development (Sinclair *et al*, 2013). To examine
277 how the loss of SLC7A5 affects B cell proliferation in response to LPS + IL-4
278 stimulation, B cells were purified from WT and *Slc7a5*$^{fl/fl}$/Vav-iCre^{+ve} mice, labelled with
279 CTV, and stimulated for 72 hours with LPS + IL-4 *ex vivo*. The percentage of viable B
280 cells after 72 hours was much lower in *Slc7a5*$^{fl/fl}$/Vav-iCre^{+ve} mice compared to WT B
281 cells (Figure 4F). Similarly, while WT B cells proliferated, the majority of the
282 *Slc7a5*$^{fl/fl}$/Vav-iCre^{+ve} B cells failed to divide, and the number of live B cells after 72
283 hours was much lower compared to WT B cells (Figure 4G, H). In line with the failure
284 to proliferate, there was no evidence of class switching in the remaining *Slc7a5*$^{fl/fl}$/Vav-
285 iCre^{+ve} B cells (Figure 4I). SLC7A5 transports large neutral amino acids, including
286 phenylalanine, histidine, methionine, tryptophan, and isoleucine, as well as the

287 tryptophan metabolite kynurenine (Fotiadis *et al*, 2013). As kynurenine is fluorescent,
288 and its uptake can be measured by flow cytometry, the effect of LPS + IL-4 treatment
289 on kynurenine uptake in B cells was determined. In line with the increased expression
290 of SLC7A5 in LPS + IL-4 treated B cells, kynurenine uptake was also higher in B cells
291 stimulated with LPS + IL-4 for 24 hours compared to naive B cells (Figure
292 4J). Kynurenine uptake in the LPS + IL-4 stimulated B cells was reduced by the
293 competitive substrate 2-aminobicyclo-(2,2,1)-heptane-2-carboxylic acid (BCH), which
294 inhibits uptake through System L transporters. Kynurenine uptake in *Slc7a5*$^{fl/fl}$/Vav-
295 iCre^{+ve} B cells was similar to the uptake in BCH-treated WT cells, suggesting that
296 SLC7A5 was the major system L transporter in LPS + IL-4 stimulated B cells (Figure
297 4J). BCH or SLC7A5 knockout did not reduce kynurenine uptake to baseline levels,
298 indicating that other transport mechanisms for kynurenine uptake exist in B cells.
299 Similar results were obtained for B cells stimulated with LPS alone, suggesting that
300 LPS rather than IL-4 is the main driver of kynurenine uptake (Figure 4K).

301

302 Cholesterol metabolism is upregulated in activated B cells

303 The enrichment analysis (Figure 1H) suggested that sterol biosynthesis may be
304 upregulated by LPS + IL-4 stimulation. Sterol biosynthesis allows the generation of
305 cholesterol from acetyl-CoA within the cell via a complex multistep process (Figure
306 S7). The 1st half of this pathway, often referred to as the mevalonate pathway, results
307 in the production of farnesyl pyrophosphate (Buhaescu & Izzedine, 2007). This can
308 be used for several purposes in the cell, including the synthesis of cholesterol via the
309 Bloch or Kandutsch-Russell pathways (Mitsche *et al*, 2015), prompting us to
310 investigate this pathway further. Analysis of the proteomic data showed that the
311 majority of enzymes involved in cholesterol biosynthesis were increased in LPS + IL-
312 4 stimulated B cells relative to naive B cells (Figure 5A). Cholesterol biosynthesis is
313 controlled by 2 rate-limiting steps: the conversion of HMG-CoA to mevalonic acid,
314 which is catalysed by HMG-CoA-reductase (HMGCR), and the conversion of squalene
315 to 2,3(*S*)-oxidosqualene, catalysed by squalene monooxygenase (SQLE) (Buhaescu
316 & Izzedine, 2007). While neither of these enzymes were detected in the proteomic
317 dataset for naive B cells, they were both consistently expressed after LPS + IL-4
318 stimulation (Figure 5B, C). Cells can also obtain cholesterol via the uptake of low-
319 density lipoprotein (LDL) through the low-density lipoprotein receptor (LDLR) (Luo *et*
320 *al*, 2020). Similar to HMGCR and SQLE, the LDLR was not found in naive B cells but
321 was detected in B cells following LPS + IL-4 stimulation (Figure 5D). Analysis of
322 published transcriptomic data (Tesi et al, 2019) on LPS stimulated B cells showed that
323 *Hmgcr*, *Sqle* and *Ldlr* mRNA expression was significantly increased by LPS
324 stimulation, and peaked after 4 hours of stimulation (Figures S6C-E).

325 Cholesterol homeostasis is regulated by the transcription factor SREBP2, which is
326 found as an immature precursor protein embedded in the endoplasmic reticulum (ER)
327 with chaperones SCAP and INSIG (Luo *et al*, 2020; Brown *et al*, 2018). Low sterol
328 levels are detected by the sterol-sensing domain of SCAP, leading to the dissociation

329 and degradation of INSIG. Subsequently, the SCAP-SREBP2 complex is transported
330 from the ER to the Golgi apparatus, where it interacts with site 1 and site 2 proteases,
331 allowing cleavage of SREBP2. The mature form of SREBP2 then translocates to the
332 nucleus, resulting in the upregulation of genes involved in cholesterol metabolism,
333 including *hmgcr*, *sqle*, and *ldlr* (Luo *et al*, 2020; Brown *et al*, 2018). Low levels of
334 SREBP2 expression were detectable in naïve B cells and became upregulated
335 following LPS + IL-4 stimulation (Figure 5E). Conversely, there was no significant
336 difference in the mRNA expression of *Srebp2* (Figure S6F), suggesting that the
337 regulation of SREBP2 levels may occur post-transcriptionally.

338 Together, the above results suggest that LPS + IL-4 stimulation would drive an
339 increase in cellular cholesterol. To test this, B cells were stained with the fluorescent
340 dye filipin, which binds to cellular cholesterol. LPS + IL-4 stimulation resulted in a
341 gradual increase in cholesterol levels from 4 hours to 24 hours of stimulation (Figure
342 5F). As cells can obtain cholesterol via *de novo* synthesis or uptake of LDL from
343 serum, we compared the effects of culturing B cells in normal serum or serum treated
344 with fumed silica to remove LDL (Brovkovych *et al*, 2019). Analysis of the serum
345 indicated that this treatment successfully removed LDL and HDL but did not affect the
346 levels of triglycerides (Table S2). Culture in media free of LDL (cholesterol-free (CF)
347 media) did not prevent the increase in filipin staining stimulated by LPS + IL-4 (Figure
348 5G-I). Inhibitors of cholesterol biosynthesis were titrated to determine what
349 concentration was required to reduce filipin staining in B cells stimulated in CF media.
350 The increase in cholesterol following LPS + IL-4 stimulation could be reduced by the
351 HMGCR inhibitor Fluvastatin or by NB-598, an inhibitor of SQLE (Figure 5G, H). Cells
352 remained viable after 24 hours of inhibitor treatment with up to 100μM of either inhibitor
353 (Figure S8A-F). Furthermore, the ability of HMGCR/SQLE inhibition to reduce
354 cholesterol levels did not correlate with effects on cell size, as judged by FSC
355 measurements by flow cytometry after 24 hours (Figure S8B, E). From this, a
356 concentration of 10μM was chosen for both NB-598 and Fluvastatin, as this was
357 sufficient to reduce cholesterol as close to naïve B cell levels as possible, but did not
358 cause significant cell death after 24 hours. Different classes of statins have been
359 described to exert different pleiotropic effects *in vivo* (Greenwood *et al*, 2006; Oesterle
360 *et al*, 2017). Depending on their solubility, statins can be categorised as hydrophilic or
361 lipophilic. Lipophilic statins, such as Fluvastatin, passively diffuse into cells, whereas
362 hydrophilic statins may enter the cell through active transport. In the case of LPS + IL-
363 4 stimulated B cells, the use of a more hydrophilic statin, Rosuvastatin, gave similar
364 results to Fluvastatin (Figure S8G-J).

365 The increase in filipin staining following LPS + IL-4 stimulation for 24 hours in normal
366 media was reduced, but not abolished, by either NB-598 or Fluvastatin treatment
367 (Figure 5I). The ability of NB-598 and Fluvastatin treatment to reduce LPS + IL-4
368 induced filipin staining was greater in CF media relative to normal media that contains
369 cholesterol (Figure 5I). Together, these results suggest that B cells may obtain
370 cholesterol via a combination of biosynthesis and uptake.

The mevalonate pathway is critical for the survival and proliferation of LPS + IL-4 stimulated B cells

As the above data indicated that B cells increased their cholesterol levels following LPS + IL-4 stimulation, we assessed the importance of this process for B cell proliferation *ex vivo.*

Stimulation with LPS + IL-4 for 48 hours in normal media promoted proliferation, and this was reduced by treatment with either Fluvastatin or NB-598 (as shown by CTV staining, Figure 6A). In line with this decreased proliferation, both Fluvastatin and NB-598 greatly reduced the number of B cells present at 48 hours compared to cells treated with LPS + IL-4 alone (Figure 6B). The remaining cells in the Fluvastatin or NB-598 treated conditions also showed significantly lower levels of survival (based on 7-AAD staining, Figure 6C) and failed to increase in size (as judged by forward scatter, Figure 6D). Similarly, B cells grown in CF media were still able to proliferate at a normal rate and experienced similar inhibitory effects after treatment with Fluvastatin or NB-598 (Figure 6A-D).

To determine if blocking cholesterol biosynthesis or cholesterol uptake induced any major changes in the proteome, we analysed splenic B cells after 24 hours of LPS + IL-4 stimulation in normal and CF media in the presence or absence of Fluvastatin, using DIA-based mass spectrometry.

Using cutoffs of a log2 fold change more than one standard deviation away from the median and $q < 0.05$, no significant changes in protein expression were found when comparing LPS + IL-4 stimulated B cells cultured in normal media to those in CF media (Figure S9A). There was an upregulation of 31 proteins and a downregulation of 12 proteins when comparing LPS + IL-4 stimulated B cells grown in normal media with and without Fluvastatin (Figure S9B). The enrichment analysis (Table S1) did not highlight any specific processes in the downregulated proteins, but the upregulated proteins were enriched in terms associated with steroid biosynthesis. This suggests Fluvastatin treatment does not cause any major off-target effects in the B cells. Comparing LPS + IL-4 stimulated B cells grown in normal media to those in CF media + Fluvastatin, there was an upregulation of 32 proteins and downregulation of 35 proteins (Figure S9C). Again, the enrichment analysis (Table S1) did not highlight any specific processes in the downregulated proteins, but there was an enrichment for proteins involved in steroid biosynthesis in the upregulated proteins. Comparing upregulated proteins from Figure SF9B and C across all the conditions indicated that for most changes, the combination of CF media and Fluvastatin had the greatest effect (Figure SF9D). A similar pattern was observed for the downregulated proteins (Figure SF9E). Looking specifically at proteins involved in cholesterol metabolism, the majority of these were upregulated by treatment with Fluvastatin or growth in CF media (Figure S9F), including the rate-limiting enzymes HMGCR and SQLE (Figure S9G, H). In addition, there was upregulation of the LDLR (Figure S9I). Again, the biggest effect on these proteins was seen with the combination of CF media and Fluvastatin.

413 In addition to cholesterol biosynthesis, the mevalonate pathway is also required for
414 protein prenylation, a process that involves the addition of a farnesyl or
415 geranylgeranyl motif to cysteine residues near the C-terminus of target proteins
416 (Figure S7) (Wang & Casey, 2016). As SQLE acts downstream of this branch point,
417 the effects of NB-598 would argue for an important role of cholesterol biosynthesis in
418 LPS + IL-4 induced proliferation; however, they would not exclude a parallel role for
419 protein prenylation. To determine if the inhibitory effects of Fluvastatin in stimulated B
420 cells may be in part due to changes in prenylation, B cells were treated with a dual
421 prenylation inhibitor, FGTI-2734 (Kazi *et al*, 2019), which blocks the enzymes
422 responsible for catalysing prenylation; farnesyl transferase (FTase) and
423 geranylgeranyl transferase (GGTase). Treatment of B cells with FGTI-2734 for 48
424 hours decreased proliferation in response to LPS + IL-4 stimulation in normal media
425 (Figure 6E), and in line with this, the number of live B cells also decreased (Figure
426 6F). Cell survival was significantly reduced to the same level as seen with
427 Fluvastatin treatment (compare Figure 6G to 6C). FGTI-2734 also had a major
428 impact on cell size in normal media (Figure 6H). Similar effects were observed in CF
429 media (Figure 6E-6H). To determine whether inhibiting farnesylation or
430 geranylgeranylation was responsible for the inhibitory effect of FGTI-2734, B cells
431 were treated with the FTase inhibitor FTI-277 (Lerner *et al*, 1995) or the GGTase
432 inhibitor GGTI-298 (McGuire *et al*, 1996). In normal media, treatment with 10μM of
433 FTI-277 reduced proliferation to around two generations of B cells (Figure 6I),
434 whereas 30μM of FTI-277 had a more significant effect on proliferation (Figure 6I).
435 Inhibition of GGTase with either 10μM or 30μM of GGTI-298 blocked proliferation
436 entirely (Figure 6I). In line with this, the number of live B cells was significantly
437 reduced by treatment with either inhibitor (Figure 6J). In terms of survival, FTI-277
438 reduced the percentage of live B cells compared to the LPS + IL-4 stimulation alone,
439 whereas GGTI-298 had a more profound impact on survival (Figure 6K). Similarly,
440 treatment with FTI-277 reduced cell size, but GGTI-298 reduced cell size to a level
441 comparable to naïve B cells (Figure 6L). Similar effects were observed in CF media
442 (Figure 6M-6P); however, treatment with GGTI-298 reduced survival to an even
443 greater extent compared to normal media (Figure 6O).

444 In theory, the effects of HMGCR inhibition should be reduced if cells were
445 supplemented with a metabolite downstream of HMGCR in the mevalonate pathway.
446 To test this, the effects of supplementing growth medium with mevalonate, the product
447 generated in the reaction catalysed by HMGCR, were tested. For this, a concentration
448 of 2mM mevalonate was used, as initial experiments showed that higher
449 concentrations resulted in cell death and reduced filipin staining (Figure S10A-
450 B). Initially, the ability of mevalonate to rescue the effects of Fluvastatin on filipin
451 staining was examined. In cells treated for 48 hours with LPS + IL-4, the reduction in
452 filipin caused by Fluvastatin treatment in normal media was reversible by the addition
453 of mevalonate (Figure 7A). Mevalonate had less effect on cells stimulated for 24 hours
454 with LPS + IL-4, although at this time point, the ability of Fluvastatin to reduce filipin
455 staining was also less pronounced than at 48 hours (Figure 7A). Surprisingly, in CF
456 media, mevalonate was unable to rescue the effects of Fluvastatin at either time point
457 (Figure 7B).

458 The effect of Fluvastatin on cell survival was partially reversible by the addition of
459 mevalonate in normal media, which restored cell survival to 80% (Figure 7C) and fully
460 restored cell size relative to cells stimulated with LPS and IL-4 in the absence of
461 Fluvastatin (Figure 7D). However, mevalonate supplementation was not sufficient to
462 completely rescue proliferation, as CTV staining demonstrated that 2 generations of B
463 cells were present rather than 4 generations after LPS + IL-4 stimulation alone (Figure
464 7E). The number of live B cells following mevalonate addition was significantly higher
465 compared to the Fluvastatin only condition, but did not reach the same level as LPS +
466 IL-4 stimulation alone (Figure 7F). Similar to what was seen for filipin staining,
467 mevalonate was unable to rescue any of the inhibitory effects of Fluvastatin treatment
468 in CF media (Figure 7C-F).

469 Since inhibiting geranylgeranyl transferase had such a profound effect on B cell
470 function, the role of prenylation was also tested by supplementing cells with
471 geranylgeranyl pyrophosphate (GGPP), which can be used for prenylation but not
472 cholesterol biosynthesis. Surprisingly, GGPP was more effective than mevalonate in
473 rescuing the effect of Fluvastatin on LPS + IL-4 induced proliferation (Figure 8A), and
474 in line with this, there was a greater number of live B cells in the GGPP treated
475 condition relative to the mevalonate treated condition (Figure 8B). A combination of
476 GGPP and mevalonate did not have a synergistic effect compared to GGPP alone
477 (Figure 8A, B). GGPP was also able to rescue the effects of Fluvastatin on both cell
478 survival and cell size (Figure 8C, D). Conversely, in CF media, the addition of GGPP
479 was unable to rescue any of the inhibitory effects of Fluvastatin on cell proliferation or
480 survival (Figure 8E-H).

481 Given that GGPP should rescue prenylation but not cholesterol metabolism, its effects
482 on proliferation were unexpected if B cells need cholesterol to proliferate. We
483 therefore tested if GGPP affected cholesterol levels in Fluvastatin treated B cells. As
484 seen in previous experiments, Fluvastatin reduced the ability of LPS + IL-4 stimulation
485 to increase cholesterol levels at both 24 hours and 48 hours of treatment. GGPP was
486 able to partially rescue this at both time points (Figure 8I). This was in contrast to
487 mevalonate, which could only rescue at 48 hours (Figure 7A), an observation that may,
488 in part, explain why GGPP was more effective at restoring proliferation in the presence
489 of Fluvastatin than mevalonate. The effects of GGPP on cholesterol levels were,
490 however, limited to normal media, as similar to mevalonate, GGPP did not rescue the
491 effect of Fluvastatin on filipin staining in CF media (Figure 8J).

492

493 MAPK and mTOR signalling are required for B cell proliferation and 494 cholesterol metabolism

495 To investigate how LPS induces these metabolic changes, we examined signalling
496 pathways activated downstream of TLR4. MyD88 is a key adaptor protein which links
497 most TLRs, including TLR4, to downstream signalling proteins (Kawai *et al*, 2024).
498 To confirm the necessity of this protein for LPS signalling, we stimulated B cells from
499 WT and MyD88 knockout (KO) mice with LPS for 30 minutes before immunoblotting

500 for the phosphorylation of downstream proteins. Knockout of MyD88 prevented the
501 phosphorylation of p38α and ERK1/2. LPS also activates PI3K/mTOR pathways in
502 B cells, and loss of Myd88 reduced the phosphorylation of AKT, p70S6K and S6 in
503 these pathways (Figure S11).

504 To determine if these signalling pathways were important for LPS-induced B cell
505 proliferation, B cells were treated with inhibitors of MAPK and mTOR signalling
506 before stimulation with LPS + IL-4 for 48 hours. B cells treated with PD184352, an
507 inhibitor of MEK1/2 (Bain *et al*, 2007), the upstream activators of ERK1/2, were still
508 able to proliferate, with 4 generations of B cells present (Figure 9A). However,
509 looking at the proportion of B cells per generation revealed that a higher percentage
510 of B cells treated with PD184352 remained in generation 1 with a smaller percentage
511 in generation 4, compared to the LPS + IL-4 stimulation alone (Figure 9B).
512 Treatment with VX745, a selective inhibitor of p38α and β (McGuire *et al*, 2013), had
513 a lesser effect on proliferation, with the only difference being a lower percentage in
514 generation 4 (Figure 9A-B). To determine the impact of inhibiting both p38/MEK1/2
515 signalling, we treated B cells with a combination of both PD184352 and VX745,
516 which reduced proliferation to 3 generations of B cells with a higher proportion of B
517 cells in generations 1 and 2 (Figure 9A, B). Inhibition of the mTOR pathway using
518 rapamycin had the greatest effect on proliferation out of all the compounds tested,
519 resulting in 70% of B cells remaining in generation 1, with few cells progressing past
520 generation 2 (Figure 9A-B). This correlated with the number of live B cells, with
521 combined MAPK inhibition and mTOR inhibition resulting in the biggest impact on B
522 cell number (Figure 9C). Interestingly, most of the inhibitor treatments had minimal
523 impact on the percentage of live cells at 48 hours, although treatment with
524 PD184352 reduced the percentage of live cells by 7% and the combination of
525 PD184352 and VX745 by 15% (Figure 9D). In terms of cell size, treatment with
526 PD184352, the combination of PD184352 and VX745, and rapamycin reduced cell
527 size (Figure 9E). Treatment with all of the inhibitors reduced the levels of filipin
528 staining, with combined PD184352 and VX745 treatment having the most significant
529 effect on cholesterol levels (Figure 9F). Together, this would suggest multiple
530 signalling pathways feed into the regulation of cholesterol in LPS activated B cells.
531 Interestingly, while the mTOR pathway is strongly linked to the regulation of protein
532 synthesis (Ma & Blenis, 2009), rapamycin reduced but did not block protein
533 synthesis and amino acid uptake in B cells stimulated with LPS + IL-4 (Figure S12A,
534 B).

535

536 The mevalonate pathway is required for B cell proliferation in response to 537 multiple agonists

538 While the above results indicate that cholesterol is required for B cell proliferation in
539 response to LPS + IL-4 stimulation, they do not demonstrate whether the primary
540 signal for this is LPS or IL-4. To test this, B cells were stimulated with either IL-4, LPS,
541 or a combination of both, and changes in cholesterol were measured by filipin staining.
542 Stimulation with either LPS or IL-4 for 24 hours was able to increase cholesterol levels,
543 although LPS had a greater effect (Figure 10A).

544 Considering the effects of HMGCR inhibition on cholesterol levels following LPS
545 stimulation, we also tested whether other stimuli known to promote B cell proliferation
546 could elevate cholesterol levels. Both the TLR7 agonist Resiquimod and the TLR9
547 agonist CpG increased cholesterol levels in B cells (Figure 10B). Similar to TLR
548 agonists, both anti-IgM and CD40L stimulation increased cholesterol levels in B cells
549 (Figure 10B). Likewise, Resiquimod, CpG, anti-IgM, and CD40L were all able to
550 stimulate proliferation, as evidenced by CTV labelling and live B cell number after 72
551 hours of treatment (Figure 10D, E). While none of these stimuli were as effective at
552 inducing proliferation as LPS, in each case, treatment with Fluvastatin reduced
553 survival and blocked proliferation of the B cells (Figure 10C-E).

554 Since stimulation with these agonists increased cholesterol levels in B cells, we
555 wondered whether that correlated with an increased expression of key proteins
556 involved in cholesterol metabolism at a proteomic level. Based on proteomic data from
557 (James *et al*, 2024) stimulation of B cells with either IL-4, anti-IgM or anti-CD40 could
558 increase levels of HMGCR, SQLE and LDLR, with the largest increase in expression
559 seen with a combination of these stimuli (Figure S13A-D).

560

561 ## Discussion

562 In this study, we have used proteomic analysis to highlight the switch in metabolic
563 demand from naïve B cells in a resting state to LPS + IL-4 activated B cells, which
564 significantly increase their energy and biosynthetic requirements to sustain growth,
565 proliferation, and class switching.

566 Upon activation, B cells upregulated several amino acid transporters, including the
567 system L transporters SLC7A5 and 6 (Figure 4A), which can import large neutral
568 amino acids, including the essential amino acids histidine, isoleucine, leucine,
569 methionine, phenylalanine, threonine, tryptophan, and valine (Fotiadis *et al*, 2013). Of
570 these 2 transporters, SLC7A5 was expressed at a higher level and was responsible
571 for the majority of amino acid uptake via system 1 transporters (Figure 4J). SLC7A5
572 forms a dimer with CD98 (SLC3A2) to form an active transporter. SLC7A5 is not,
573 however, the only binding partner of CD98, as it can also bind to the SLC7A11 and
574 SLC7A6 transporters or interact with integrins (Kahya *et al*, 2021). Previous work has
575 shown that mice with B cell-specific deletions of CD98 presented normal development
576 of B cells in the bone marrow, but significantly lower levels of class-switched IgG due
577 to the inhibition of B cell proliferation and plasma cell formation following the activation
578 of naive B cells in the periphery (Cantor *et al*, 2009). The defect in proliferation was
579 attributed to defective integrin signalling rather than an impairment in amino acid
580 transport, based on the deletion of the integrin or amino acid transporter regions in
581 CD98. Knockout of SLC7A5 in either hematopoietic cells or B cells has been
582 previously shown not to affect the number of splenic B cells in mice (Sinclair *et al*,
583 2013), although a separate study found a decrease in the number of peritoneal B1
584 cells (Sun *et al*, 2023). While not critical for initial B cell development, SLC7A5 was

585 critical for the survival and expansion of B cells in response to *ex vivo* stimulation with
586 LPS + IL-4 (Figure 4F-I). Of note, recent research in human B cells has shown that
587 stimulation with CpG increases SLC7A5 expression, which in turn transports L-leucine
588 into the cell and facilitates mTORC activation, which was required for IgG production
589 and inflammatory cytokine secretion (Torigoe *et al*, 2019).

590 Similar observations have been made in T cells, where SLC7A5 is not required for
591 initial T cell development but is required for the clonal expansion and effector functions
592 of T cells following activation via the T cell receptor in the periphery (Sinclair *et al*,
593 2013). This suggests that B cells, similar to T cells, may rely on different amino acid
594 transporters at different points in their development. The expression of SLC7A5
595 following T cell activation has been shown to require the transcription factor c-Myc
596 (Marchingo *et al*, 2020). While the role of c-Myc was not directly addressed in this
597 study, analysis of the proteomic data presented here does show that c-Myc was
598 increased by LPS stimulation (Table S3). This is consistent with previous reports
599 showing an upregulation of c-Myc in response to several B cell activating stimuli,
600 including LPS, CD40, and the BCR (Luo *et al*, 2018; Dominguez-Sola *et al*, 2012;
601 Calado *et al*, 2012; Tesi *et al*, 2019). While in T cells, c-Myc regulates metabolic
602 changes, including the expression of SLC7A5 (Sinclair & Cantrell, 2025), this has not
603 been studied to the same degree in B cells. Of note, transcriptional profiling following
604 LPS stimulation of B cells has suggested that SLCA5 mRNA induction in response to
605 LPS can occur in the absence of c-Myc (Tesi *et al*, 2019), suggesting that the
606 regulation of SLC7A5 may not be identical between T and B cells.

607 As B cells expand and divide, they will require an increase in lipids to generate new
608 membrane. Cholesterol is an important lipid component of the plasma membrane,
609 which affects membrane fluidity (Luo *et al*, 2020) and has also been implicated in the
610 regulation of several receptors, including the BCR (Bléry *et al*, 2006). The regulation
611 of cholesterol levels in cells is therefore closely controlled at the level of both
612 cholesterol biosynthesis and its uptake via the endocytosis of LDL particles. Low
613 levels of cholesterol in the endoplasmic reticulum are detected by the transcription
614 factor SREBP2 (Luo *et al*, 2020; Brown *et al*, 2018). The importance of this system in
615 B cells was recently demonstrated by the conditional knockout of SCAP in B cells, a
616 key regulator of SREBP1 and 2. While this did not prevent the development of B cells
617 or their levels at steady state in mice, it did prevent the activation and proliferation of
618 B cells in response to antigens and thus compromised the humoral immune
619 response. SCAP deletion will, however, affect both SREBP1 and SREBP2 function
620 and therefore have wider effects on lipid metabolism beyond its effects on
621 cholesterol. We show here that in response to several activating stimuli *ex vivo*,
622 including LPS, B cells upregulate cholesterol, and that blocking HMGCR, a key rate-
623 limiting enzyme in the cholesterol biosynthesis pathway, inhibits B cell proliferation
624 (Figure 10B-E). In the case of LPS stimulation, B cells seem to be able to obtain
625 cholesterol by both uptake and biosynthesis. For example, B cells can still increase
626 their cholesterol levels in the absence of LDL in the cell culture medium (Figure 5I). In
627 addition, NB-598, an inhibitor of the 2nd rate-limiting enzyme in the cholesterol

628 biosynthesis pathway, can reduce the ability of LPS to increase cholesterol levels
629 (Figure 5I). In contrast, the greater effect of NB-598 on cholesterol levels of B cells
630 grown in CF media relative to normal media (Figure 5I), and the inability of mevalonate
631 to rescue the effects of statin treatment in CF media (Figure 7B-F), would indicate that
632 B cells also use LDL uptake as a source of cholesterol. In line with this, B cells
633 upregulated the LDLR following activation (Figure 5D). Additionally, proteomic analysis
634 of LPS + IL-4 stimulated B cells grown in normal vs CF media, or +/- Fluvastatin
635 treatment (normal) reveals an upregulation of proteins involved in cholesterol
636 metabolism, including HMGCR, SQLE and LDLR (Figure S9). This suggests that a
637 feedback mechanism exists whereby the detection of low cholesterol levels (either due
638 to blocking biosynthesis or uptake) by SREBP2 increases the expression of
639 cholesterol metabolic proteins. A similar study in activated CD8+ T cells has
640 demonstrated that knockout of the LDLR leads to an upregulation of proteins involved
641 in cholesterol biosynthesis, including HMGCR, and a reduction in proteins involved in
642 cholesterol efflux compared to WT CD8+ T cells (Bonacina *et al*, 2022). The precise
643 balance between these two mechanisms in B cells may depend on the duration of
644 stimulation and the availability of LDL in the extracellular environment.

645 In line with our results, following CD40 mediated activation of human B cells,
646 Atorvastatin was reported to inhibit human B cell proliferation and the expression of
647 the activation markers CD80 and CD86 (Shimabukuro-Vornhagen *et al*, 2014).
648 Interpretation of the effects of statins on B cells is, however, complex. Statins inhibit
649 HMGCR, the rate-limiting enzyme in the mevalonate pathway that is required for the
650 initial steps in cholesterol biosynthesis. This pathway generates farnesyl
651 pyrophosphate, an intermediate that can feed into not only cholesterol biosynthesis,
652 but also protein prenylation and ubiquinone pathways (Mullen *et al*, 2016; Wang &
653 Casey, 2016). Thus, the effects of statins reported here could be due not only to their
654 effects on cholesterol, but also via these other pathways. Prenylation has been linked
655 to proliferation in several cell types (Su *et al*, 2020), including T cells, where
656 Simvastatin inhibits activation via two mechanisms, one of which involves blocking the
657 prenylation of Ras and Rac (Ghittoni *et al*, 2005). We therefore investigated whether
658 statin-mediated effects on B cell survival and proliferation were in part due to
659 prenylation. We found that FGTI-2734, a dual inhibitor of FTase and GGTase, blocked
660 LPS + IL-4 induced B cell proliferation and survival (Figure 6E-H). Similar GGTI-298,
661 an inhibitor of GGTase, had a stronger inhibitory effect on B cell function compared to
662 FTI-277, which blocks FTase activity, suggesting an important role for prenylation in B
663 cells (Figure 6I-P). In agreement with this, prenylation has also been reported to be
664 important in B cells for the expression of CD80 and CD86 following stimulation via
665 CD40, although its role in proliferation was not directly addressed (Shimabukuro-
666 Vornhagen *et al*, 2014). Given that prenylation can target a large number of proteins,
667 including many members of the Ras GTPase superfamily, to regulate their cellular
668 localisation, the effects of blocking prenylation in B cells are likely to be complex.
669 Interestingly, GGPP, which is needed for protein geranylgeranylation, was able to
670 rescue the effects of Fluvastatin on LPS + IL-4 stimulated B cells in normal media

671 (Figure 8A-D). Notably, it was more efficient than mevalonate at restoring proliferation
672 in the Fluvastatin treated B cells. This ability to rescue proliferation was unexpected,
673 as GGPP would not directly feed into the cholesterol biosynthesis pathway, and other
674 experiments described here using CF media and squalene monooxygenase inhibitors
675 argue for a requirement of cholesterol for B cell proliferation. We therefore looked at
676 its effect on cholesterol levels and found that GGPP was able to rescue the effects of
677 Fluvastatin in normal but not CF media (Figure 8I,J). This could be explained by
678 prenylation being required for cholesterol uptake but not biosynthesis. Cholesterol
679 uptake via the LDLR requires the clathrin-mediated endocytosis of the LDLR and its
680 trafficking to endosomes, where cholesterol is released from LDL (Nguyen *et al*,
681 2025). Vesicle trafficking is regulated via the action of several Rab GTPases, including
682 Rab5, which is recruited to early endosomes and regulates their maturation (Zhao *et*
683 *al*, 2025; Zeigerer *et al*, 2012). More significantly, Rab5 prenylation has been shown
684 to be important for its correct targeting to endosomes, and therefore its biological
685 function (Gomes *et al*, 2003). Treatment of cells with statins to inhibit prenylation has
686 previously been shown to affect Rab subcellular localisation and vesicle trafficking (Ali
687 *et al*, 2010; Ronzier *et al*, 2019; Xia *et al*, 2018). Loss of the prenylation of Rab
688 proteins involved in LDLR endocytosis could therefore negatively impact this process,
689 leading to a failure of LDL uptake into the B cell. Prenylation is also likely to impact
690 other processes in B cells, for example, TLR9-induced IL-10 production by regulatory
691 B cells has been found to require geranylgeranylation and not farnesylation (Bibby *et*
692 *al*, 2020). Further work will be necessary to identify the proteins prenylated upon B
693 cell activation and to determine the effects of prenylation on their function.

694 In terms of the pathways that control B cell function downstream of TLR4 signalling,
695 we found that inhibition of p38α/β and MEK1/2 signalling impacted B cell growth and
696 proliferation, as well as cholesterol levels (Figure 9A-F). Related to this, inhibition of
697 MEK1/2 has been found to abolish *LDLR* promoter activity (Kotzka *et al*, 2000), and
698 depletion of ERK2, but not ERK1, significantly reduced the expression levels of
699 *SREBP2*, *HMGCR* and *LDLR* (Yu *et al*, 2019). Studies in primary mouse
700 hepatocytes have demonstrated that treatment with the p38α/β inhibitor SB203580
701 also significantly reduced *LDLR* promoter activity (Pham *et al*, 2016).

702 Additionally, we found that blocking mTOR had a major inhibitory effect on B cell
703 proliferation (Figure 9A-B), as well as reducing cholesterol levels (Figure 9F), and to
704 a lesser extent, the rate of protein synthesis and amino acid uptake through System
705 L transporters (Figure 12A-B). In response to environmental cues, including energy
706 and nutrient availability, the mTORC1 complex regulates processes such as cell
707 growth and proliferation (Saxton & Sabatini, 2017). Previous studies have shown that
708 the addition of amino acids to the growth medium increases the transcription of
709 genes involved in cholesterol biosynthesis, including HMGCR and SREBP2 (Eid *et*
710 *al*, 2017). Treatment with the mTORC1 inhibitor Torin1 blocked this effect,
711 suggesting that cholesterol metabolism may be dependent on mTORC1 activity (Eid
712 *et al*, 2017).

713 Overall, the proteomic analysis described here supports that B cells undergo a major
714 reorganisation of metabolic pathways following TLR activation. Naïve B cells exist in
715 a quiescent state where they do not grow or proliferate and express low levels of
716 metabolic enzymes. Conversely, B cells stimulated with LPS + IL-4 massively
717 upregulate metabolic enzymes involved in processes including protein synthesis,
718 amino acid uptake, and cholesterol metabolism, which is required to support an
719 increase in cell size, proliferation, and antibody class switching. Most significantly, we
720 found that LPS + IL-4 stimulated B cells depended on cholesterol biosynthesis,
721 cholesterol uptake, and prenylation for expansion and proliferation.

722

723 Methods

724 Mice

725 Wildtype C57BL/6 mice (Charles Rivers) aged between 8 and 12 weeks were used
726 for the majority of experiments. Conditional *SLC7A5* knockout mice bred to Vav-iCre
727 mice have been described previously and were maintained on a C57Bl6/J
728 background (de Boer *et al*, 2003; Poncet *et al*, 2014; Sinclair *et al*, 2013). MyD88
729 knockout mice have been described previously and were maintained on a C57Bl6/J
730 background (Adachi et al, 1998). The mice were kept in individually ventilated cages
731 under specific pathogen-free conditions. Mice were given free access to food (RM3
732 irradiated pelleted diet, Special Diet Services) and water. Animal rooms were
733 maintained at 21°C and a humidity of 45 to 55% with a 12/12 h light cycle. Mice were
734 sacrificed using a rising concentration of CO_2, and death was confirmed by either
735 cervical dislocation or exsanguination. All animal work was approved by the
736 University of Dundee's Welfare and Ethical Use of Animals Committee and in
737 accordance with UK and EU law.

738

739 Cell isolation

740 Lymph nodes were homogenised through a 40µM cell strainer in DPBS buffer (Gibco),
741 and after centrifugation at 450g for 4 minutes, the pellet was resuspended in DPBS.
742 Lymphocytes were counted on a Novocyte (Agilent Technologies) and seeded at
743 1×10^6 cells/ml in B cell medium (RPMI-1640 supplemented with 10% FBS, 50 U/ml
744 penicillin-streptomycin, 5mM L-glutamine, 10mM HEPES buffer, 1mM sodium
745 pyruvate, 50 µM 2-mercaptoethanol and non-essential amino acids) for stimulation.

746 Spleens were dissociated through a 40µM filter in DPBS buffer, and after centrifugation
747 at 450g for 4 minutes, the pellet was resuspended in 1ml of Red Blood Cell Lysing
748 Buffer (Hybri-Max™, Sigma) for 4 minutes at room temperature to lyse red blood cells.
749 The reaction was quenched by the addition of DPBS, and the cells were pelleted by
750 centrifugation at 450g for 4 minutes. The pellet was resuspended in 10ml DPBS before
751 counting the splenocytes on a Novocyte. Splenocytes were seeded at 1×10^6 cells/ml
752 in B cell medium for stimulation or used for further purification of B cells.

753 ## B cell isolation

754 To obtain an enriched population of B cells, magnetic sorting was used to remove non-
755 B cells. Briefly, splenocytes were incubated with Fc receptor-blocking anti-CD16/CD32
756 antibody (BD Pharmingen) for 5 minutes on ice. The cells were incubated with a
757 mixture of biotin-labelled anti-mouse antibodies (10µg/ml) (Table 1) for 20 minutes on
758 ice. Unbound antibody was removed by washing with 10ml Magnetic Activated Cell
759 Sorting (MACS) buffer (DPBS + 0.5% BSA + 2mM EDTA), followed by centrifugation.
760 The cells were then resuspended in MACS buffer with streptavidin microbeads (1:10)
761 (Miltenyi Biotech) and incubated at 4ºC for 15 minutes. Miltenyi LD columns were
762 calibrated by passing through 3ml of MACS buffer. Cells were washed with 10ml
763 MACS buffer and centrifuged at 450g for 4 minutes to remove excess beads. The cell
764 pellet was then resuspended in MACS buffer and separated using magnetic-activated
765 cell sorting columns (LD) according to the manufacturer's instructions (Miltenyi
766 Biotec). Single-cell suspensions were collected, and B cell numbers and purity
767 (CD19+) were measured on a NovoCyte. Typical purity levels were 97% CD19+ B
768 cells. B cells were seeded at 2×10^5 cells/ml of B cell medium for stimulation for flow
769 cytometry experiments unless otherwise stated. When stated, purified B cells were
770 stained with 2.5µM CellTrace™ Violet (ThermoFisher) at 37ºC for 20 minutes, then
771 quenched in 10ml B cell medium before seeding at the required density.

772

773 ## Stimulations and inhibitors

774 Cells were rested at 37ºC for 1 hour. When required, the cells were pre-treated with
775 the appropriate inhibitor (Table 2) for 45 minutes before stimulation, at the
776 concentrations indicated in the figure legend. Inhibitors were dissolved in DMSO
777 (Thermo Fisher) and used at a dilution of 1:1000 of culture medium. As indicated in
778 the figure legends, cells were treated with 1µl DMSO as a vehicle control.
779
780 Cells were pre-incubated with the following metabolites at 37ºC for 1 hour before
781 inhibitor treatment/stimulation. Metabolites were used at the concentrations indicated
782 in the figure legend: Mevalonic acid 5-phosphate lithium salt hydrate (Sigma Aldrich),
783 which was dissolved in HEPES (Thermo Fisher). As indicated in the figure legends,
784 cells were treated with 20µl HEPES as a vehicle control. Geranylgeranyl
785 pyrophosphate ammonium salt (Sigma Aldrich), which comes in a 7:3 methanol:
786 ammonium hydroxide solution. As indicated in the figure legends, cells were treated
787 with 4.55µl 7:3 methanol: ammonium hydroxide solution as a vehicle control.

788 A combination of 20µg/ml LPS (L2654, Sigma) and 10ng/ml IL-4 (214-14, Peprotech)
789 was used to stimulate the cells unless otherwise stated in the figure legend. For some
790 experiments, cells were treated with LPS or IL-4 alone, or with 1µg/ml
791 Resiquimod/R848 (tlrl-r848, Invivogen), 1µg/ml ODN 2006 (tlrl-2006, Invivogen),
792 10µg/ml Anti-Mouse IgM µ chain (115-006-075, Stratech) or 500ng/ml CD40 ligand
793 (8230-CL-050/CF, R&D).

Cholesterol free serum.

Silica-depleted FBS was purchased from Biowest and used in place of normal FBS when making B cell culture medium. Samples of normal and cholesterol-free FBS were sent to London Health Company, which carried out tests to measure changes in triglycerides, cholesterol, high-density lipoprotein (HDL) and low-density lipoprotein (LDL) (Table S2).

Cell survival, proliferation and class switching assays

Following stimulation, cells were washed in Fluorescence Activated Cell Sorting (FACS) buffer (1% BSA, DPBS) and then incubated with Fc receptor-blocking anti-CD16/CD32 antibody in FACS buffer for 15 minutes at 4ºC before staining with the appropriate fluorochrome-conjugated antibodies (Table 3) in FACS buffer for 20 minutes at 4ºC. The samples were washed with FACS buffer prior to resuspension in 0.25µg of 7AAD. Flow cytometry data was collected on a Novocyte and analysed using FlowJo V.10 software (BD Biosciences). A representative gating strategy is shown in Figure S14A for lymph node/splenocyte isolation, and Figure S15B for B cell isolation.

p-STAT1 staining

Splenocytes (1×10^6 cells/ml) were stimulated with LPS (20µg/ml) and/or IFN-β for 15 minutes before washing in FACS buffer. The cells were fixed using 1:1 IC fixation buffer (catalogue number: 00-8222-49, eBiosciences) in FACS buffer and incubated at room temperature for 20 minutes. Following another wash in FACS buffer, cells were resuspended in 100µl of cold ethanol and stored at -20ºC for 30 minutes. The samples were washed with FACS buffer twice before incubation with Fc receptor-blocking anti-CD16/CD32 antibody in FACS buffer for 15 minutes at 4ºC. The cells were incubated with p-STAT1 (Table 4) for 1 hour at room temperature before washing with FACS buffer and incubation with (1:1000) anti-rabbit IgG (H+L), $F(ab')_2$ Fragment (Alexa Fluor® 647 Conjugate) (Cell Signalling Technology, 4414S) and CD19 PE (Table 3) for 1 hour at room temperature. The cells were washed with FACS buffer before resuspension in 300µl FACS buffer. Flow cytometry data was collected on a Novocyte and analysed using FlowJo V.10 software.

Cell cycle analysis and p-Rb staining

Cells were washed in FACS buffer and then fixed using 1:1 IC fixation buffer and FACS buffer, and incubated at room temperature for 20 minutes. Following another wash in FACS buffer, cells were resuspended in 100µl of cold ethanol and stored at -20ºC for 30 minutes. The samples were washed with FACS buffer twice before incubation with Fc receptor-blocking anti-CD16/CD32 antibody in FACS buffer for 15 minutes at 4ºC. Surface stains (Table 3) were incubated for 1 hour at room temperature before washing with FACS buffer and resuspension in 0.5µg/ml of DAPI. Flow cytometry data

834 was collected on a Novocyte and analysed using FlowJo V.10 software. A
835 representative gating strategy is shown in Figure S14B.

836

837 O-propargyl-puromycin uptake assay

838 Uptake of the puromycin analogue O-propargyl-puromycin was used to estimate
839 protein synthesis rates. Splenocytes (1×10^5 cells/100µl) were stimulated with 20µg/ml
840 LPS and 10ng/ml IL-4. After 24 hours, the cells were treated with 20µM of O-propargyl-
841 puromycin for 30 minutes at 37ºC. 100µl of 2% paraformaldehyde in B cell medium
842 was added to the cells before incubation in complete darkness at room temperature
843 for 30 minutes. The samples were pelleted by centrifugation at 450g for 4 minutes
844 before resuspension in 100µl of DPBS. Following this, the samples were washed with
845 FACS buffer and then resuspended in 100µl of 0.01% Saponin (Sigma) in DPBS,
846 before incubation at room temperature for 20 minutes. The samples were pelleted by
847 centrifugation at 450g for 4 minutes before resuspension in 30µl of Click mixture: 1mM
848 Copper sulphate (209198, Sigma), 10mM Sodium ascorbate (A7631. Sigma), 1mM
849 BTTAA (906328, Sigma), 10mM Aminoguanidine (81530, Cayman Chemicals), DPBS
850 (14190144, Gibco), 5µM Alexafluor 647 azide (A10277, Invitrogen) and incubation in
851 complete darkness at room temperature for 1 hour. The samples were pelleted by
852 centrifugation at 450g for 4 minutes before resuspension in 200µl of FACS buffer and
853 incubation in complete darkness at room temperature for 30 minutes. Again, the
854 samples were pelleted by centrifugation at 450g for 4 minutes before washing again
855 in FACS buffer. The cells were incubated with Fc receptor-blocking anti-CD16/CD32
856 antibody in FACS buffer for 15 minutes at 4ºC. Surface stains (Table 3) were incubated
857 for 1 hour at room temperature. The samples were washed with FACS buffer prior to
858 resuspension in 300µl FACS buffer. Flow cytometry data was collected on a Novocyte
859 and analysed using FlowJo V.10 software. A representative gating strategy is shown
860 in Figure S14C.

861

862 Kynurenine uptake assay

863 Uptake of the tryptophan metabolite kynurenine was used to estimate the uptake rates
864 via neutral amino acid transporters (Sinclair *et al*, 2018). Purified B cells (1×10^6
865 cells/ml) were stimulated with 20µg/ml LPS and 10ng/ml IL-4. For the assay, pre-warm
866 HBSS, BCH (40mM in HBSS) and Kynurenine (800µM in HBSS) to 37ºC. After 24
867 hours, the cells were washed in FACS buffer and then incubated with Fc receptor-
868 blocking anti-CD16/CD32 antibody in FACS buffer for 15 minutes at 37ºC before
869 staining with CD19 APC (Table 3) in FACS buffer for 20 minutes at 37ºC. The samples
870 were washed with FACS buffer and then resuspended in 200µl HBSS. Keep the
871 samples at 37ºC. Either 100µl of HBSS or 100µl of BCH was then added to each
872 sample. After this, 100µl of Kynurenine was added, and the samples were incubated
873 for 5 minutes at 37ºC. After 5 minutes, the samples were fixed by adding 125µl of 4%
874 paraformaldehyde made in DPBS for 30 minutes at room temperature. The samples

875 were then washed 2 times with FACS buffer and re-suspended in 400µl of FACS buffer.
876 Flow cytometry data was collected on an LSR Fortessa (BD biosciences) and
877 analysed using FlowJo V.10 software. A representative gating strategy is shown in
878 Figure S14D.

879

880 Cholesterol staining assay

881 Changes in cellular cholesterol content were determined using the cholesterol-binding
882 agent filipin (Miller, 1984). Splenocytes were stimulated with 20µg/ml LPS and 10ng/ml
883 IL-4. After 24 hours, the cells were washed twice in DPBS before staining for viability
884 using eFluor 660 fixable viability dye (Table 3) for 30 minutes at 4ºC. After two washes
885 in FACS buffer, the cells were fixed using 1:1 IC fixation buffer and FACS buffer, before
886 incubation at 4ºC for 20 minutes. Following another wash in FACS buffer, cells were
887 incubated with Fc receptor-blocking anti-CD16/CD32 antibody in FACS buffer for 15
888 minutes at 4ºC. Surface stains (Table 3) were incubated for 20 minutes at 4ºC. The
889 samples were washed with FACS buffer prior to resuspension in 270µl FACS buffer
890 and 30µl of 1µg/µl filipin (Merck) before incubation in complete darkness at room
891 temperature for 30 minutes. Flow cytometry data was collected on an LSR Fortessa
892 and analysed using FlowJo V.10 software. A representative gating strategy is shown
893 in Figure S15A.

894

895 Mitochondria staining assay

896 Splenocytes were stimulated with 20µg/ml LPS and 10ng/ml IL-4. After 24 hours, the
897 cells were washed twice in FACS buffer. 50µl of prewarmed (37°C) staining solution
898 containing 100nM MitoTracker Red probe (Invitrogen) in FACS buffer was added to
899 the cells before incubation at 37°C for 20 minutes. The samples were washed with
900 FACS buffer before incubation with Fc receptor-blocking anti-CD16/CD32 antibody
901 (BD Pharmingen) in FACS buffer for 15 minutes at 4ºC before staining with the
902 appropriate fluorochrome-conjugated antibodies (Table 3) in FACS buffer for 20
903 minutes at 4ºC. The samples were washed with FACS buffer prior to resuspension in
904 0.25µg of 7AAD. Flow cytometry data was collected on a Novocyte and analysed using
905 FlowJo V.10 software. A representative gating strategy is shown in Figure S15C.

906

907 Immunoblotting

908 B cells were seeded at $2x10^6$ cells/ml of B cell medium for immunoblotting. To
909 generate lysates, the cells were stimulated with LPS (20µg/ml) for 60 minutes and
910 centrifuged at 100g for 2 minutes. The pellet was resuspended in 300µl of SDS
911 Triton Lysis buffer (50mM Tris-HCL pH 7.5, 1% (v/v) Triton-X-100, 1mM EGTA, 1mM
912 EDTA, 1mM Sodium Orthovanadate, 50mM Sodium fluoride, 1mM Sodium
913 Pyrophosphate, 10mM Sodium B-glycerophosphate, 0.27M Sucrose, 0.1% (v/v) 2-β-
914 mercatoethanol, cOmplete mini EDTA-Free Protease Inhibitor, 1% Sodium Dodecyl

915 sulfate, 5% Glycerol) and incubated for 5 minutes at 100ºC to denature proteins.
916 Following a brief period of cooling, the DNA was sheared using a 25g syringe and
917 the samples were stored at -20ºC. Cell lysates were resolved by SDS-PAGE using
918 10% gels in running buffer (250mM Tris, 1% (w/v) 10% Sodium Dodecyl Sulfate,
919 192mM glycine) and transferred to nitrocellulose membranes in the presence of
920 transfer buffer (48 mM Tris, 39 mM glycine, 20% (v/v) methanol). The membranes
921 were blocked using 5% (w/v) skimmed milk powder (Marvel) in TBST (0.5M Tris-HCl,
922 pH 7.6, 1.5M NaCl and 0.1%(v/v) Tween 20). Primary antibodies (Table 4) were used
923 at a dilution of 1/1000 overnight in TBST with 5% (w/v) BSA. The membranes were
924 incubated with Anti-rabbit HRP (horseradish peroxidase) secondary antibodies
925 (Sigma) in 5% (w/v) milk powder in TBST. The blots were developed with Clarity™
926 Western ECL substrate (Bio-Rad) and scanned using Li-Cor Odyssey Fc Imager
927 (Licor) (Chemi, 600nm and 700nm channels). Image Studio software was utilised to
928 compile Western blot data.
929

930 ## Proteomics

931 For the naïve vs LPS + IL-4 dataset, wildtype C57BL/6 mice (Charles Rivers) aged
932 between 8 and 12 weeks were used for all proteomic experiments. Lymph nodes were
933 extracted from mice, mashed in RPMI media before filtering through a 70µm cell
934 strainer. Naïve B cells were purified by fluorescence-activated cell sorting.
935 Lymphocytes were incubated with Fc receptor-blocking anti-CD16/CD32 antibody (BD
936 Pharmingen) in FACS buffer for 15 minutes at 4ºC before staining with fluorochrome-
937 conjugated antibodies (Table 3) in FACS buffer for 20 minutes at 4ºC. The samples
938 were washed with FACS buffer prior to resuspension in 0.5µg/ml of DAPI. CD19+,
939 CD93-, DAPI- cells were sorted using a Sony SH800 cell sorter. Sorted cells were
940 washed twice with HBSS and snap frozen in liquid nitrogen to be stored at -80 °C until
941 processing for mass spectrometry. For B cell activation, lymphocytes were suspended
942 at a final density of 1.5 million cells/ml in medium (RPMI-1640 containing glutamine
943 supplemented with 10% FBS, 50 U/ml penicillin-streptomycin, 50 µM 2-
944 mercaptoethanol) and activated for 24 hours in the presence of 20µg/ml LPS and
945 10ng/ml IL-4. After 24 hours, the cells were incubated with Fc receptor-blocking anti-
946 CD16/CD32 antibody (BD Pharmingen) in FACS buffer for 15 minutes at 4ºC before
947 staining with fluorochrome-conjugated antibodies (Table 3) in FACS buffer for 20
948 minutes at 4ºC. The samples were washed with FACS buffer prior to resuspension in
949 0.5µg/ml of DAPI. CD19+ and DAPI- were sorted and collected as described above.
950 Cells were then washed 3 times in PBS and cell pellets frozen at -80°C.

951 For the dataset in Figure S9, B cells were isolated from murine spleens as described
952 above and seeded at 2×10^5 cells/ml of B cell medium, with 1×10^6 cells/5ml per
953 condition. Cells were rested at 37ºC for 1 hour. Cells were washed twice with PBS and
954 snap frozen in liquid nitrogen to be stored at -80°C until processing for mass
955 spectrometry. For activation, B cells were pre-treated with Fluvastatin (10µM) for 45
956 minutes before stimulation. The cells were stimulated with LPS (20µg/ml) and IL-4

957 (10ng/ml) for 24 hours. Cells were washed twice with PBS and snap frozen in liquid
958 nitrogen to be stored at -80 °C until processing for mass spectrometry.

959 Cell pellets were lysed, and proteins were digested following the protocol described
960 by (Baker *et al*, 2022). In brief, 400 ml of lysis buffer (5% sodium dodecyl sulfate, 50
961 mM triethylammonium bicarbonate (pH 8.5) and 10 mM tris(2-carboxyethyl)
962 phosphine-hydrochloride) was added to each sample and the lysates were shaken at
963 room temperature at 1000 rpm for 5 minutes before being incubated at 95 °C at 500
964 rpm for 5 minutes. Samples were allowed to cool and were then sonicated using a
965 BioRuptor (15 cycles: 30 sec on and 30 sec off) and alkylated with 20mM
966 iodoacetamide for 1 h at 22 °C in the dark. To determine protein concentration, the
967 EZQ protein quantitation kit (Thermo) was used, and protein cleanup and digestion
968 were performed using S-TRAP mini columns (Protifi). Proteins were digested with
969 trypsin at 1:20 ratio (enzyme:protein) for 2 hours at 47°C. Digested peptides were
970 eluted from S-TRAP columns using 50mM ammonium bicarbonate, followed by 0.2%
971 aqueous formic acid and 50% aqueous acetonitrile containing 0.2% formic acid.
972 Peptides were dried by speedvac before resuspending in 1% formic acid. Peptide
973 quantity was measured using the CBQCA kit (Thermo).
974

975 ## LC-MS/MS analysis

976 Naïve vs LPS + IL-4 dataset

977 Peptides were analysed by single-shot Data Independent Acquisition (DIA) mass
978 spectrometry as previously described (Molina-Gonzalez *et al*, 2023; Sollberger *et al*,
979 2024). 1.5 µg of peptide from each sample was injected onto a nanoscale C18 reverse-
980 phase chromatography system (UltiMate 3000 RSLC nano, Thermo Scientific) and
981 electrosprayed into an Orbitrap Exploris 480 Mass Spectrometer (Thermo Fisher). The
982 following buffers were used for liquid chromatography: buffer A (0.1% formic acid in
983 Milli-Q water (v/v)) and buffer B (80% acetonitrile and 0.1% formic acid in Milli-Q water
984 (v/v). Samples were loaded at 10µl/min onto a trap column (100µm × 2 cm, PepMap
985 nanoViper C18 column, 5µm, 100 Å, Thermo Scientific) equilibrated in 0.1%
986 trifluoroacetic acid (TFA). The trap column was washed for 3 min at the same flow rate
987 with 0.1% TFA, then switched in-line with a Thermo Scientific, resolving C18 column
988 (75µm × 50 cm, PepMap RSLC C18 column, 2µm, 100 Å). Peptides were eluted from
989 the column at a constant flow rate of 300nl/min with a linear gradient from 3% buffer
990 B to 6% buffer B in 5 min, then from 6% buffer B to 35% buffer B in 115 min, and finally
991 to 80% buffer B within 7 min. The column was then washed with 80% buffer B for 4
992 min and re-equilibrated in 3% buffer B for 15 min. Two blanks were run between each
993 sample to reduce carryover. The column was kept at a constant temperature of 50°C.

994 The data was acquired using an easy spray source operated in positive mode with
995 spray voltage at 2.445 kV, and the ion transfer tube temperature at 250°C. The MS
996 was operated in DIA mode. A scan cycle comprised a full MS scan (m/z range from
997 350 to 1650), with RF lens at 40%, AGC target set to custom, normalised AGC target
998 at 300%, maximum injection time mode set to custom, maximum injection time at 20

ms, microscan set to 1 and source fragmentation disabled. MS survey scan was followed by MS/MS DIA scan events using the following parameters: multiplex ions set to false, collision energy mode set to stepped, collision energy type set to normalized, HCD collision energies set to 25.5, 27 and 30%, orbitrap resolution 30,000, first mass 200, RF lens 40%, AGC target set to custom, normalized AGC target 3000%, microscan set to 1 and maximum injection time 55ms. Data for both MS scan and MS/MS DIA scan events were acquired in profile mode.

Naïve vs LPS + IL-4 (Normal/CF +/- Fluvastatin)

Peptides were analysed using single-shot Data Independent Acquisition (DIA). For each sample 200ng of peptide was injected onto a C18 reverse-phase chromatography system (Vanquish, Thermo Scientific) and electrosprayed into an Astral Orbitrap Mass Spectrometer (Thermo Fisher). The following buffers were used for liquid chromatography: buffer A (0.1% formic acid in Milli-Q water (v/v)) and buffer B (80% acetonitrile and 0.1% formic acid in Milli-Q water (v/v). Samples were loaded onto a trap column (Pep Map Neo C18, 5µm, 300µm x5 mm) Thermo Scientific) equilibrated in buffer A. The column (Pep MAP RSLC C18, 2µm, 150 µm x15 cm) was equilibrated with 4% buffer and peptides were eluted at a variable flow rate, starting at 1.3 µl/min to 0.8 µl/min from 4% buffer B to 8% buffer B in 0.1 min, then from 8% buffer B to 22.5% buffer B in 13 min, and from 22.5% b to 35% B in 6.90 min. The low rate is increased from 0.8 µl/min to 2 µl/min in 0.4 min with buffer B increasing from 35% to 55%. The column is finally washed at a flow of 2µl/min with 99% buffer B. The column was kept at a constant temperature of 50°C. The data was acquired using an easy spray source operated in positive mode with spray voltage at 2.0 kV, and the ion transfer tube temperature at 280°C. The MS was operated in DIA mode. A scan cycle comprised a full MS scan (m/z range from 380-980), with orbitrap resolution at 2400000, RF lens at 40%, AGC target set to custom, normalised AGC target at 500%, absolute AGC value set to 5.00e6, maximum injection time 5ms and micros-can set to 1. MS survey scan was followed by MS/MS DIA scan events using the following parameters: DIA window type set to auto, isolation window 2, window overlap set to 0, window placement optimisation on, number of scan events 299, collision energy type normalized, HCD collision energy 25%, detector type Astral, scan range 150-2000, normalized AGC target 500%, absolute AGC target 5.000e4, maximum injection time 5 ms, microscan set to 1, loop

control time, time 0.6s. Data for both MS scan and MS/MS DIA scan events were acquired in profile mode.

Proteomic data analysis

For comparing naïve and stimulated B cells, raw mass spec data files were searched using Spectronaut version 19 (Biognosys). Data was analysed by DirectDIA. Raw mass spec data files were searched against a mouse database (Swissprot Trembl November 2023) with the following parameters: directDIA, false discovery rate set to 1%, protein N-terminal acetylation and methionine oxidation were set as variable modifications and carbamidomethylation of cysteine residues was selected as a fixed modification.

The following Spectronaut settings were used (Baker *et al*, 2024): all identification settings were set to 0.01 (precursor q-value cut-off, precursor PEP cut-off, protein FDR strategy (accurate), protein q-value cut-off (experiment), protein q-value cut-off (run) and protein PEP cut-off). The following quantification settings were used: ‘Quant 2.0’, the MS-Level quantity was set to ‘MS2’, imputation was disabled, major group Top N and minor group Top N were set as ‘False’ and cross run normalisation was set as ‘False’.

Intensity values from Spectronaut were further analysed in Perseus (Tyanova *et al*, 2016) and the histone ruler method (Wiśniewski *et al*, 2014) used to estimate copy number and concentrations of the identified proteins. Fold change was calculated relative to levels in naïve B cells and significance determined using unpaired Student's t tests on log10-transformed data (Table S3 and Table S4). The False Discovery Rate approach using the 2-stage step up method, Benjamini, Krieger, and Yekutieli (Benjamini *et al*, 2006) with a Q value of 0.01 (Table S3). Enrichment against the Gene Ontology (GO) Biological Processes, Uniprot Keyword Biological Process and *Kyoto Encyclopaedia of Genes and Genomes* (KEGG) databases. Biological Process GO terms (Gene Ontology Consortium *et al*, 2023) and KEGG pathways (Kanehisa *et al*, 2016) was carried out using the DAVID gene enrichment site (Sherman *et al*, 2022) (Table S1).

Statistical analysis

Unless otherwise stated, graphs show mean values + SD with individual replicates shown by symbols. Unpaired two-tailed Student’s *t* test, one-way ANOVA, two-way ANOVA with post-hoc testing were performed in Prism, and the tests used are indicated in the figure legends. Full results of the ANOVA calculations are given in Supplemental Table S5.

Table 1: MACS antibodies				
Antibody	Clone	Concentration	Catalogue number	Supplier
Anti-CD11b	M1/70	10μg/ml	101204	BioLegend
Anti-CD11c	N418	10μg/ml	117304	BioLegend
Anti-CD3ε	145-2C11	10μg/ml	100304	BioLegend
Anti-TER119	TER-119	10μg/ml	116204	BioLegend

1071

Table 2: Inhibitors				
Name	Target	Concentration	Catalogue number	Supplier
Fluvastatin sodium	HMG-CoA reductase	0.1μM -100μM	3309	Tocris
Rosuvastatin calcium	HMG-CoA reductase	0.1μM -100μM	6343	Tocris
NB-598	Squalene monooxygenase	0.1μM -100μM	HY-16343	MedChem Express
FGTI-2734	Farnesyl and gerany lgeranyl transferase-1	10μM	HY-128350	MedChem Express
FTI-277 hydrochloride	Farnesyl transferase	10μM-30μM	HY-15872A	MedChem Express
GGTI-289 trifluoroacetate	Geranylgeranyl transferase-1	10μM-30μM	HY-15871	MedChem Express
PD18352	MSK1/2	2μM	4237	Tocris
VX745	P38	1μM	3915	Tocris
Rapamycin	mTOR	20nM	R8781	Merck

1072

Table 3: Flow cytometry antibodies					
Antibody	Fluorophore	Clone	Dilution	Catalogue number	Supplier
Anti-CD19	APC	6D5	1:300	115512	Biolegend
Anti-CD19	PE	1D3	1:200	557399	BD Biosciences
Anti-CD19	FITC	1D3	1:200	152403	BioLegend
Anti-CD93	APC	AA4.1	1:200	136510	BioLegend
Anti-CD98	PE	RL388	1:200	128208	BioLegend
dsDNA	eFluor 660	-	1:1000	65-0864-14	eBioscience
Anti-IgG1	FITC	A85-1	1:100	553443	BD Biosciences
Anti-pRb	FITC	D20B12	1:300	4277S	Cell Signaling Technology

1073

1074

Table 4: Western blot primary antibodies				
Antibody target	Animal raised in	Dilution	Code	Source
Phospho-STAT1 (Tyr701)	Rabbit	1:1000	9167	Cell Signalling Technology
Phospho-p44/42 MAPK (Erk1/2) (Thr202/Tyr204)	Rabbit	1:1000	9101	Cell Signalling Technology
p44/42 MAPK (Erk1/2)	Rabbit	1:1000	9102	Cell Signalling Technology
Phospho-p38 MAPK (Thr180/Tyr182)	Rabbit	1:1000	4511	Cell Signalling Technology
p38 MAPK	Rabbit	1:1000	9212	Cell Signalling Technology
Phospho-Akt (Ser473)	Rabbit	1:1000	4060	Cell Signalling Technology
Phospho-p70 S6 Kinase (Thr389)	Rabbit	1:1000	9234	Cell Signalling Technology
Phospho-S6 Ribosomal Protein (Ser235/236)	Rabbit	1:1000	2211	Cell Signalling Technology
S6 Ribosomal Protein (5G10)	Rabbit	1:1000	2217	Cell Signalling Technology

1075

1076

1077 ## Acknowledgments

1078 The authors thank A. Rennie and R. Clarke from the Flow Cytometry Facility for cell
1079 sorting and advice on flow cytometry. We also thank the FingerPrints Proteomics
1080 facility for running our samples for mass spectrometry and for advice on proteomics.
1081 This research was supported by a Wellcome Trust (DMSC, UNS148487) and MRC
1082 (MR/N013735/1, MR) PhD studentship awards.

1083

1084 ## Author contributions

1085 D.M.S.C., M.R., S.A., performed the experiments. A.J.M. performed the liquid
1086 chromatography–mass spectrometry. D.M.S.C and J.S.C.A analysed the proteomics
1087 data. L.V.S designed the kynurenine uptake and protein synthesis experiments. M.S
1088 optimised the silica depletion and filipin staining experiments. D.M.S.C and J.S.C.A
1089 wrote the manuscript.

Declaration of interests

The authors declare no competing interests or disclosures.

For the purpose of open access, the author has applied a Creative Commons Attribution (CC BY) licence to any Author Accepted Manuscript version arising from this submission.

Resource availability

Lead contact

Further information and requests for resources should be directed to and will be fulfilled by the lead contact, Simon Arthur (j.s.c.arthur@dundee.ac.uk).

Materials availability

This study did not generate any new unique reagents.

Data availability

The mass spectrometry proteomics data (Naïve vs LPS + IL-4) has been deposited to the ProteomeXchange Consortium (http://proteomecentral.proteomexchange.org) via the PRIDE partner repository (Perez-Riverol *et al*, 2024) with the dataset identifier PXD057739.

The mass spectrometry proteomics data (Naïve vs LPS + IL-4 (Normal/CF) +/- Fluvastatin has been deposited to PRIDE with the dataset identifier PXD074568

Flow cytometry data that support the findings of this study are available from the corresponding author upon request. Any additional information required to reanalyse the data reported in this paper is available from the lead contact upon request.

Supplemental information

Document S1. Figures S1–S16, Table S2 - Serum tests related to Figure 5 and Table S5 - Statistics table related to all figures.

Supplemental Table S1. Excel file containing terms for protein enrichment too large to fit in a pdf. Related to Figure 1H.

Supplemental Table S3. Excel file containing proteomic data set (Naïve vs LPS + IL-4)

Supplemental Table S4. Excel file containing proteomic data set (Naïve vs LPS + IL-4 (Normal/CF +/- Fluvastatin)

References

Adachi O, Kawai T, Takeda K, Matsumoto M, Tsutsui H, Sakagami M, Nakanishi K & Akira S (1998) Targeted Disruption of the MyD88 Gene Results in Loss of IL-1- and IL-18-Mediated Function. Immunity 9: 143–150

Ali BR, Nouvel I, Leung KF, Hume AN & Seabra MC (2010) A novel statin-mediated "prenylation block-and-release" assay provides insight into the membrane targeting mechanisms of small GTPases. *Biochemical and Biophysical Research Communications* 397: 34–41

Arthur JSC & Ley SC (2013) Mitogen-activated protein kinases in innate immunity. *Nat Rev Immunol* 13: 679–692

Arunkumar N, Liu C, Hang H & Song W (2013) Toll-like receptor agonists induce apoptosis in mouse B-cell lymphoma cells by altering NF-κB activation. *Cell Mol Immunol* 10: 360–372

Bain J, Plater L, Elliott M, Shpiro N, Hastie CJ, McLauchlan H, Klevernic I, Arthur JSC, Alessi DR & Cohen P (2007) The selectivity of protein kinase inhibitors: a further update. *Biochem J* 408: 297–315

Baker CP, Bruderer R, Abbott J, Arthur JSC & Brenes AJ (2024) Optimizing Spectronaut Search Parameters to Improve Data Quality with Minimal Proteome Coverage Reductions in DIA Analyses of Heterogeneous Samples. *J Proteome Res* 23: 1926–1936

Baker CP, Phair IR, Brenes AJ, Atrih A, Ryan DG, Bruderer R, Dinkova-Kostova AT, Lamont DJ, Arthur JSC & Howden AJM (2022) DIA label-free proteomic analysis of murine bone-marrow-derived macrophages. *STAR Protocols* 3: 101725

Barberis M, Klipp E, Vanoni M & Alberghina L (2007) Cell Size at S Phase Initiation: An Emergent Property of the G1/S Network. *PLOS Computational Biology* 3: e64

Benjamini Y, Krieger AM & Yekutieli D (2006) Adaptive linear step-up procedures that control the false discovery rate. *Biometrika* 93: 491–507

Bibby JA, Purvis HA, Hayday T, Chandra A, Okkenhaug K, Rosenzweig S, Aksentijevich I, Wood M, Lachmann HJ, Kemper C, *et al* (2020) Cholesterol metabolism drives regulatory B cell IL-10 through provision of geranylgeranyl pyrophosphate. *Nat Commun* 11: 3412

Bierling TEH, Gumann A, Ottmann SR, Schulz SR, Weckwerth L, Thomas J, Gessner A, Wichert M, Kuwert F, Rost F, *et al* (2024) GLUT1-mediated glucose import in B cells is critical for anaplerotic balance and humoral immunity. *Cell Reports* 43: 113739

1159 Bléry M, Tze L, Miosge LA, Jun JE & Goodnow CC (2006) Essential role of membrane
1160 cholesterol in accelerated BCR internalization and uncoupling from NF-κB in B cell
1161 clonal anergy. *J Exp Med* 203: 1773–1783

1162 Bonacina F, Moregola A, Svecla M, Coe D, Uboldi P, Fraire S, Beretta S, Beretta G,
1163 Pellegatta F, Catapano AL, *et al* (2022) The low-density lipoprotein receptor–mTORC1
1164 axis coordinates CD8+ T cell activation. *The Journal of Cell Biology* 221: e202202011

1165 de Boer J, Williams A, Skavdis G, Harker N, Coles M, Tolaini M, Norton T, Williams K,
1166 Roderick K, Potocnik AJ, *et al* (2003) Transgenic mice with hematopoietic and
1167 lymphoid specific expression of Cre. *Eur J Immunol* 33: 314–325

1168 Brookens SK, Cho SH, Paik Y, Meyer K, Raybuck AL, Park C, Greenwood DL,
1169 Rathmell JC & Boothby MR (2023) Plasma Cell Differentiation, Antibody Quality, and
1170 Initial Germinal Center B Cell Population Depend on Glucose Influx Rate. *The Journal*
1171 *of Immunology* 212: 43–56

1172 Brovkovych V, Aldrich A, Li N, Atilla-Gokcumen GE & Frasor J (2019) Removal of
1173 Serum Lipids and Lipid-Derived Metabolites to Investigate Breast Cancer Cell Biology.
1174 *PROTEOMICS* 19: 1800370

1175 Brown MS, Radhakrishnan A & Goldstein JL (2018) Retrospective on Cholesterol
1176 Homeostasis: The Central Role of Scap. *Annu Rev Biochem* 87: 783–807

1177 Buhaescu I & Izzedine H (2007) Mevalonate pathway: A review of clinical and
1178 therapeutical implications. *Clinical Biochemistry* 40: 575–584

1179 Calado DP, Sasaki Y, Godinho SA, Pellerin A, Köchert K, Sleckman BP, de Alborán IM,
1180 Janz M, Rodig S & Rajewsky K (2012) The cell-cycle regulator c-Myc is essential for
1181 the formation and maintenance of germinal centers. *Nat Immunol* 13: 1092–1100

1182 Cantor J, Browne CD, Ruppert R, Féral CC, Fässler R, Rickert RC & Ginsberg MH
1183 (2009) CD98hc facilitates B cell proliferation and adaptive humoral immunity. *Nat*
1184 *Immunol* 10: 412–419

1185 Chicas A, Wang X, Zhang C, McCurrach M, Zhao Z, Mert O, Dickins RA, Narita M,
1186 Zhang M & Lowe SW (2010) Dissecting the unique role of the retinoblastoma tumor
1187 suppressor during cellular senescence. *Cancer Cell* 17: 376–387

1188 Coutinho A, Gronowicz E, Bullock WW & Möller G (1974) MECHANISM OF THYMUS-
1189 INDEPENDENT IMMUNOCYTE TRIGGERING. *The Journal of Experimental*
1190 *Medicine* 139: 74–92

1191 D'Avola A, Legrave N, Tajan M, Chakravarty P, Shearer RL, King HW, Kluckova K,
1192 Cheung EC, Clear AJ, Gunawan AS, *et al* (2022) PHGDH is required for germinal
1193 center formation and is a therapeutic target in MYC-driven lymphoma. *J Clin Invest*
1194 132: e153436

1195 Dominguez-Sola D, Victora GD, Ying CY, Phan RT, Saito M, Nussenzweig MC & Dalla-
1196 Favera R (2012) The proto-oncogene MYC is required for selection in the germinal
1197 center and cyclic reentry. *Nat Immunol* 13: 1083–1091

Doudna JA & Rath VL (2002) Structure and Function of the Eukaryotic Ribosome: The Next Frontier. *Cell* 109: 153–156

Dufort FJ, Bleiman BF, Gumina MR, Blair D, Wagner DJ, Roberts MF, Abu-Amer Y & Chiles TC (2007) Cutting Edge: IL-4-Mediated Protection of Primary B Lymphocytes from Apoptosis via Stat6-Dependent Regulation of Glycolytic Metabolism1. *The Journal of Immunology* 179: 4953–4957

Dziarski R (1982) Preferential induction of autoantibody secretion in polyclonal activation by peptidoglycan and lipopolysaccharide. I. In vitro studies. *The Journal of Immunology* 128: 1018–1025

Eid W, Dauner K, Courtney KC, Gagnon A, Parks RJ, Sorisky A & Zha X (2017) mTORC1 activates SREBP-2 by suppressing cholesterol trafficking to lysosomes in mammalian cells. *Proc Natl Acad Sci* 114: 7999–8004

Engeland K (2022) Cell cycle regulation: p53-p21-RB signaling. *Cell Death Differ* 29: 946–960

Fotiadis D, Kanai Y & Palacín M (2013) The SLC3 and SLC7 families of amino acid transporters. *Molecular Aspects of Medicine* 34: 139–158

Gene Ontology Consortium, Aleksander SA, Balhoff J, Carbon S, Cherry JM, Drabkin HJ, Ebert D, Feuermann M, Gaudet P, Harris NL, *et al* (2023) The Gene Ontology knowledgebase in 2023. *Genetics* 224: iyad031

Genestier L, Taillardet M, Mondiere P, Gheit H, Bella C & Defrance T (2007) TLR Agonists Selectively Promote Terminal Plasma Cell Differentiation of B Cell Subsets Specialized in Thymus-Independent Responses1. *The Journal of Immunology* 178: 7779–7786

Ghittoni R, Patrussi L, Pirozzi K, Pellegrini M, Lazzerini PE, Capecchi PL, Pasini FL & Baldari CT (2005) Simvastatin inhibits T-cell activation by selectively impairing the function of Ras superfamily GTPases. *The FASEB Journal* 19: 1–24

Gomes AQ, Ali BR, Ramalho JS, Godfrey RF, Barral DC, Hume AN & Seabra MC (2003) Membrane Targeting of Rab GTPases Is Influenced by the Prenylation Motif. *Mol Biol Cell* 14: 1882–1899

Greenwood J, Steinman L & Zamvil SS (2006) Statin therapy and autoimmune disease: from protein prenylation to immunomodulation. *Nat Rev Immunol* 6: 358–370 Hodgkin PD, Lee JH & Lyons AB (1996) B cell differentiation and isotype switching is related to division cycle number. *Journal of Experimental Medicine* 184: 277–281

Hoffman W, Lakkis FG & Chalasani G (2016) B Cells, Antibodies, and More. *Clinical Journal of the American Society of Nephrology* 11: 137

Hoshino K, Takeuchi O, Kawai T, Sanjo H, Ogawa T, Takeda Y, Takeda K & Akira S (1999) Cutting Edge: Toll-Like Receptor 4 (TLR4)-Deficient Mice Are Hyporesponsive to Lipopolysaccharide: Evidence for TLR4 as the Lps Gene Product1. *The Journal of Immunology* 162: 3749–3752

Howden AJM, Hukelmann JL, Brenes A, Spinelli L, Sinclair LV, Lamond AI & Cantrell DA (2019) Quantitative analysis of T cell proteomes and environmental sensors during T cell differentiation. *Nat Immunol* 20: 1542–1554

Iwata TN, Ramírez-Komo JA, Park H & Iritani BM (2017) Control of B lymphocyte development and functions by the mTOR signaling pathways. *Cytokine & Growth Factor Reviews* 35: 47–62

James O, Sinclair LV, Lefter N, Salerno F, Brenes A & Howden AJM (2024) A proteomic map of B cell activation and its shaping by mTORC1, MYC and iron. 2024.12.19.629506 doi:10.1101/2024.12.19.629506 [PREPRINT]

Jellusova J, Cato MH, Apgar JR, Ramezani-Rad P, Leung CR, Chen C, Richardson AD, Conner EM, Benschop RJ, Woodgett JR, *et al* (2017) Gsk3 is a metabolic checkpoint regulator in B cells. *Nat Immunol* 18: 303–312

Johnson AG, Gaines S & Landy M (1956) Studies on the O antigen of Salmonella typhosa. V. Enhancement of antibody response to protein antigens by the purified lipopolysaccharide. *The Journal of experimental medicine* 103: 225–246

Johnstone JC, Yazicioglu YF & Clarke AJ (2024) Fuelling B cells: dynamic regulation of B cell metabolism. *Current Opinion in Immunology* 91: 102484 Kahya U, Köseer AS & Dubrovska A (2021) Amino Acid Transporters on the Guard of Cell Genome and Epigenome. *Cancers* 13: 125

Kanehisa M, Sato Y, Kawashima M, Furumichi M & Tanabe M (2016) KEGG as a reference resource for gene and protein annotation. *Nucleic Acids Res* 44: D457-462

Kawai T, Adachi O, Ogawa T, Takeda K & Akira S (1999) Unresponsiveness of MyD88-Deficient Mice to Endotoxin. *Immunity* 11: 115–122

Kawai T, Ikegawa M, Ori D & Akira S (2024) Decoding Toll-like receptors: Recent insights and perspectives in innate immunity. *Immunity* 57: 649–673

Kazi A, Xiang S, Yang H, Chen L, Kennedy P, Ayaz M, Fletcher S, Cummings C, Lawrence HR, Beato F, *et al* (2019) Dual Farnesyl and Geranylgeranyl Transferase Inhibitor Thwarts Mutant KRAS-Driven Patient-Derived Pancreatic Tumors. *Clinical Cancer Research* 25: 5984–5996

Kotzka J, Müller-Wieland D, Roth G, Kremer L, Munck M, Schürmann S, Knebel B & Krone W (2000) Sterol regulatory element binding proteins (SREBP)-1a and SREBP-2 are linked to the MAP-kinase cascade. *J Lipid Res* 41: 99–108

Leone G, DeGregori J, Yan Z, Jakoi L, Ishida S, Williams RS & Nevins JR (1998) E2F3 activity is regulated during the cell cycle and is required for the induction of S phase. *Genes Dev* 12: 2120–2130

Lerner EC, Qian Y, Blaskovich MA, Fossum RD, Vogt A, Sun J, Cox AD, Der CJ, Hamilton AD & Sebti SM (1995) Ras CAAX peptidomimetic FTI-277 selectively blocks oncogenic Ras signaling by inducing cytoplasmic accumulation of inactive Ras-Raf complexes. *J Biol Chem* 270: 26802–26806

Luo J, Yang H & Song B-L (2020) Mechanisms and regulation of cholesterol homeostasis. *Nat Rev Mol Cell Biol* 21: 225–245

Luo W, Weisel F & Shlomchik MJ (2018) B Cell Receptor and CD40 Signaling Are Rewired for Synergistic Induction of the c-Myc Transcription Factor in Germinal Center B Cells. *Immunity* 48: 313-326.e5

Ma XM & Blenis J (2009) Molecular mechanisms of mTOR-mediated translational control. *Nat Rev Mol Cell Biol* 10: 307–318

Marchingo JM, Sinclair LV, Howden AJ & Cantrell DA (2020) Quantitative analysis of how Myc controls T cell proteomes and metabolic pathways during T cell activation. *eLife* 9: e53725

McGuire TF, Qian Y, Vogt A, Hamilton AD & Sebti SM (1996) Platelet-derived growth factor receptor tyrosine phosphorylation requires protein geranylgeranylation but not farnesylation. *J Biol Chem* 271: 27402–27407

McGuire VA, Gray A, Monk CE, Santos SG, Lee K, Aubareda A, Crowe J, Ronkina N, Schwermann J, Batty IH, *et al* (2013) Cross Talk between the Akt and p38α Pathways in Macrophages Downstream of Toll-Like Receptor Signaling. *Mol Cell Biol* 33: 4152–4165

Miller RG (1984) The use and abuse of filipin to localize cholesterol in membranes. *Cell Biol Int Rep* 8: 519–535

Mitsche MA, McDonald JG, Hobbs HH & Cohen JC (2015) Flux analysis of cholesterol biosynthesis in vivo reveals multiple tissue and cell-type specific pathways. *eLife* 4: e07999

Molina-Gonzalez I, Holloway RK, Jiwaji Z, Dando O, Kent SA, Emelianova K, Lloyd AF, Forbes LH, Mahmood A, Skripuletz T, *et al* (2023) Astrocyte-oligodendrocyte interaction regulates central nervous system regeneration. *Nat Commun* 14: 3372

Mostafavi S, Yoshida H, Moodley D, LeBoité H, Rothamel K, Raj T, Ye CJ, Chevrier N, Zhang S-Y, Feng T, *et al* (2016) Parsing the Interferon Transcriptional Network and Its Disease Associations. *Cell* 164: 564–578

Mullen PJ, Yu R, Longo J, Archer MC & Penn LZ (2016) The interplay between cell signalling and the mevalonate pathway in cancer. *Nat Rev Cancer* 16: 718–731

Napolitano L, Scalise M, Galluccio M, Pochini L, Albanese LM & Indiveri C (2015) LAT1 is the transport competent unit of the LAT1/CD98 heterodimeric amino acid transporter. *Int J Biochem Cell Biol* 67: 25–33

Nguyen MKL, Pinkenburg C, Du JJ, Bernaus-Esqué M, Enrich C, Rentero C & Grewal T (2025) The multiple facets of Rab proteins modulating the cellular distribution of cholesterol from the late endosomal compartment. *Biochimica et Biophysica Acta (BBA) - Molecular Cell Research* 1872: 119896

Obukhanych TV & Nussenzweig MC (2006) T-independent type II immune responses generate memory B cells. *Journal of Experimental Medicine* 203: 305–310

Oesterle A, Laufs U & Liao JK (2017) Pleiotropic Effects of Statins on the Cardiovascular System. *Circulation Research* 120: 229–243

Paradoski BT, Hou S, Mejia EM, Olayinka-Adefemi F, Fowke D, Hatch GM, Saleem A, Banerji V, Hay N, Zeng H, *et al* (2024) PI3K-dependent reprogramming of hexokinase isoforms controls glucose metabolism and functional responses of B lymphocytes. *iScience* 27

Pasare C & Medzhitov R (2005) Control of B-cell responses by Toll-like receptors. *Nature* 438: 364–368

Peeters R & Jellusova J (2023) Lipid metabolism in B cell biology. *Molecular Oncology.* 18(7):1795-1813

Perez-Riverol Y, Bandla C, Kundu DJ, Kamatchinathan S, Bai J, Hewapathirana S, John NS, Prakash A, Walzer M, Wang S, *et al* (2024) The PRIDE database at 20 years: 2025 update. *Nucleic Acids Res*: gkae1011

Pham DD, Do HT, Bruelle C, Kukkonen JP, Eriksson O, Mogollón I, Korhonen LT, Arumäe U & Lindholm D (2016) p75 Neurotrophin Receptor Signaling Activates Sterol Regulatory Element-binding Protein-2 in Hepatocyte Cells via p38 Mitogen-activated Protein Kinase and Caspase-3. *J Biol Chem* 291: 10747–10758

Platanias LC (2005) Mechanisms of type-I- and type-II-interferon-mediated signalling. *Nat Rev Immunol* 5: 375–386

Poltorak A, He X, Smirnova I, Liu MY, Van Huffel C, Du X, Birdwell D, Alejos E, Silva M, Galanos C, *et al* (1998) Defective LPS signaling in C3H/HeJ and C57BL/10ScCr mice: mutations in Tlr4 gene. *Science* 282: 2085–2088

Poncet N, Mitchell FE, Ibrahim AFM, McGuire VA, English G, Arthur JSC, Shi Y-B & Taylor PM (2014) The catalytic subunit of the system L1 amino acid transporter (slc7a5) facilitates nutrient signalling in mouse skeletal muscle. *PLoS One* 9: e89547

Procaccini C, Carbone F, Di Silvestre D, Brambilla F, De Rosa V, Galgani M, Faicchia D, Marone G, Tramontano D, Corona M, *et al* (2016) The Proteomic Landscape of Human Ex Vivo Regulatory and Conventional T Cells Reveals Specific Metabolic Requirements. *Immunity* 44: 406–421

Raybuck AL, Cho SH, Li J, Rogers MC, Lee K, Williams CL, Shlomchik M, Thomas JW, Chen J, Williams JV, *et al* (2018) B Cell–Intrinsic mTORC1 Promotes Germinal Center–Defining Transcription Factor Gene Expression, Somatic Hypermutation, and Memory B Cell Generation in Humoral Immunity. *J Immunol* 200: 2627–2639

Ronzier E, Parks XX, Qudsi H & Lopes CM (2019) Statin-specific inhibition of Rab-GTPase regulates cPKC-mediated IKs internalization. *Sci Rep* 9: 17747

Rubin SM, Sage J & Skotheim JM (2020) Integrating Old and New Paradigms of G1/S Control. *Mol Cell* 80: 183–192

Saxton RA & Sabatini DM (2017) mTOR Signaling in Growth, Metabolism, and Disease. *Cell* 168: 960–976

Sherman BT, Hao M, Qiu J, Jiao X, Baseler MW, Lane HC, Imamichi T & Chang W (2022) DAVID: a web server for functional enrichment analysis and functional annotation of gene lists (2021 update). *Nucleic Acids Res* 50: W216–W221

Shimabukuro-Vornhagen A, Zoghi S, Liebig TM, Wennhold K, Chemitz J, Draube A, Kochanek M, Blaschke F, Pallasch C, Holtick U, *et al* (2014) Inhibition of Protein Geranylgeranylation Specifically Interferes with CD40-Dependent B Cell Activation, Resulting in a Reduced Capacity To Induce T Cell Immunity. *The Journal of Immunology* 193: 5294–5305

Sinclair LV & Cantrell DA (2025) Protein Synthesis and Metabolism in T Cells. *Annu Rev Immunol* 43: 343–366

Sinclair LV, Neyens D, Ramsay G, Taylor PM & Cantrell DA (2018) Single cell analysis of kynurenine and System L amino acid transport in T cells. *Nat Commun* 9: 1981

Sinclair LV, Rolf J, Emslie E, Shi Y-B, Taylor PM & Cantrell DA (2013) Control of amino-acid transport by antigen receptors coordinates the metabolic reprogramming essential for T cell differentiation. *Nat Immunol* 14: 500–508

Snapper CM, Finkelman FD, Stefany D, Conrad DH & Paul WE (1988) IL-4 induces co-expression of intrinsic membrane IgG1 and IgE by murine B cells stimulated with lipopolysaccharide. *The Journal of Immunology* 141: 489–498

Sollberger G, Brenes AJ, Warner J, Arthur JSC & Howden AJM (2024) Quantitative proteomics reveals tissue-specific, infection-induced and species-specific neutrophil protein signatures. *Sci Rep* 14: 5966

Su W, Chapman NM, Wei J, Zeng H, Dhungana Y, Shi H, Saravia J, Zhou P, Long L, Rankin S, *et al* (2020) Protein Prenylation Drives Discrete Signaling Programs for the Differentiation and Maintenance of Effector Treg Cells. *Cell Metabolism* 32: 996-1011.e7

Sun Y, Wen J, Xu T & Meng L (2023) Reduction of peritoneal cavity B1a cells in adult Slc7a5 knockdown mice via dysregulating the mTOR pathway. *Int Immunopharmacol* 117: 109939

Tan H, Yang K, Li Y, Shaw TI, Wang Y, Blanco DB, Wang X, Cho J-H, Wang H, Rankin S, *et al* (2017) Integrative Proteomics and Phosphoproteomics Profiling Reveals Dynamic Signaling Networks and Bioenergetics Pathways Underlying T Cell Activation. *Immunity* 46: 488–503

Tanner LB, Goglia AG, Wei MH, Sehgal T, Parsons LR, Park JO, White E, Toettcher JE & Rabinowitz JD (2018) Four Key Steps Control Glycolytic Flux in Mammalian Cells. *Cell Syst* 7: 49-62.e8

Tesi A, de Pretis S, Furlan M, Filipuzzi M, Morelli MJ, Andronache A, Doni M, Verrecchia A, Pelizzola M, Amati B, *et al* (2019) An early Myc-dependent

transcriptional program orchestrates cell growth during B-cell activation. *EMBO reports* 20: e47987

Torigoe M, Maeshima K, Ozaki T, Omura Y, Gotoh K, Tanaka Y, Ishii K & Shibata H (2019) l-Leucine influx through Slc7a5 regulates inflammatory responses of human B cells via mammalian target of rapamycin complex 1 signaling. *Modern Rheumatology* 29: 885–891

Tyanova S, Temu T, Sinitcyn P, Carlson A, Hein MY, Geiger T, Mann M & Cox J (2016) The Perseus computational platform for comprehensive analysis of (prote)omics data. *Nat Methods* 13: 731–740

Wagner EF, Hleb M, Hanna N & Sharma S (1998) A pivotal role of cyclin D3 and cyclin-dependent kinase inhibitor p27 in the regulation of IL-2-, IL-4-, or IL-10-mediated human B cell proliferation. *J Immunol* 161: 1123–1131

Wang M & Casey PJ (2016) Protein prenylation: unique fats make their mark on biology. *Nat Rev Mol Cell Biol* 17: 110–122

Waters LR, Ahsan FM, Wolf DM, Shirihai O & Teitell MA (2018) Initial B Cell Activation Induces Metabolic Reprogramming and Mitochondrial Remodeling. *iScience* 5: 99–109

Weeratna RD, Makinen SR, McCluskie MJ & Davis HL (2005) TLR agonists as vaccine adjuvants: comparison of CpG ODN and Resiquimod (R-848). *Vaccine* 23: 5263–5270

Wiśniewski JR, Hein MY, Cox J & Mann M (2014) A “Proteomic Ruler” for Protein Copy Number and Concentration Estimation without Spike-in Standards *. *Molecular & Cellular Proteomics* 13: 3497–3506

Xia Y, Xie Y, Yu Z, Xiao H, Jiang G, Zhou X, Yang Y, Li X, Zhao M, Li L, *et al* (2018) The Mevalonate Pathway Is a Druggable Target for Vaccine Adjuvant Discovery. *Cell* 175: 1059-1073.e21

Yi A-K, Chang M, Peckham DW, Krieg AM & Ashman RF (1998) CpG Oligodeoxyribonucleotides Rescue Mature Spleen B Cells from Spontaneous Apoptosis and Promote Cell Cycle Entry1. *The Journal of Immunology* 160: 5898–5906

Yu H, Rimbert A, Palmer AE, Toyohara T, Xia Y, Xia F, Ferreira LMR, Chen Z, Chen T, Loaiza N, *et al* (2019) GPR146 Deficiency Protects Against Hypercholesterolemia and Atherosclerosis. *Cell* 179: 1276-1288.e14

Zeigerer A, Gilleron J, Bogorad RL, Marsico G, Nonaka H, Seifert S, Epstein-Barash H, Kuchimanchi S, Peng CG, Ruda VM, *et al* (2012) Rab5 is necessary for the biogenesis of the endolysosomal system in vivo. *Nature* 485: 465–470

Zhao X, Long S, Zhu M, Hao H, Liao Y, Zhang C & Liu Z (2025) Potential Roles of SNX17, Rab11, and Rab5 in LDLR Recycling. *Arteriosclerosis, Thrombosis, and Vascular Biology* 45: e338–e354

Figure Legends

Figure 1. Stimulation with LPS + IL-4 promotes B cell proliferation and class switch recombination

(A-D) Cells from the lymph nodes of C57BL6/J mice were stained with Cell Trace Violet (CTV) and stimulated with IL-4 (10ng/ml) +/- LPS (20µg/ml) for 72 hours and analysed by flow cytometry. Data for naive B cells (stained on day 0) is also shown. Live CD19+ B cells were identified using the gating strategy described in Figure S14A. **(A)** Representative flow cytometry plots comparing IgG1 expression and CTV staining after 72 hours of IL-4 or LPS + IL-4 stimulation. **(B)** Representative plots for FSC and SSC at 72 hours of IL-4 or LPS + IL-4 stimulation with geometric means for the **(C)** forward scatter and **(D)** side scatter. Data shows the results of three biological replicates. Data was analysed by one-way ANOVA followed by multiple comparison testing via Sidak's analysis. For comparisons to naïve B cells, $p<0.0001$ is indicated by ****. Full ANOVA results are given in Supplementary Table S5.

(E-H) Cells from the lymph nodes of C57BL6/J mice, stimulated with LPS (20µg/ml) and IL-4 (10ng/ml) for 24 hours, and CD19+ B cells were isolated by FACS. Alternatively, naïve CD19+ B cells were sorted directly from *ex vivo* lymph node cells. Cells were lysed and analysed by proteomics as described in the methods. Samples from four mice for LPS + IL-4 and three for naive were generated. **(E)** Total protein content (pg/cell) was estimated from the proteomic data. Statistical power was determined using an unpaired two-tailed Student's t-test, where $p<0.01$ is indicated by **. **(F)** Volcano plot depicting changes in estimated protein copy number in naïve vs LPS + IL-4 stimulated B cells. **(G)** Volcano plot showing the estimated cellular protein concentration (µM) in naïve vs LPS + IL-4 stimulated B cells. Horizontal dashed lines indicate $q<0.05$. Vertical dashed lines indicate $\log_2$ fold change of one standard deviation away from the median. **(H)** Enrichment analysis of the upregulated proteins in **(G)** against GO-term and KEGG databases.

1465 **Figure 2. Proteins involved in cell cycle progression are upregulated in LPS +**
1466 **IL-4 activated B cells**

1467 **(A-B)** B cells were purified from the spleens of C57BL6/J mice and either fixed on
1468 isolation (naive) or stimulated with LPS (20µg/ml) and IL-4 (10ng/ml) for 24 hours
1469 before fixation. Cells were then stained with DAPI and CD19. The cell cycle stages
1470 were analysed using the gating strategy shown in Figure S14B. **(A)** Representative
1471 histograms showing the proportion of B cells in different phases of the cell cycle. **(B)**
1472 Quantification shows three technical replicates from cells isolated from one mouse and
1473 is representative of three independent experiments. Statistical power was determined
1474 using two-way ANOVA followed by multiple comparison testing via Sidak's analysis,
1475 where $p<0.01$ is indicated by **, $p<0.001$ by *** and $p<0.0001$ by **** for comparisons
1476 between the naive and LPS + IL-4 conditions.

1477 **(C-F)** Graphs depicting changes in the estimated cellular concentration (nM) of
1478 proteins implicated in entry into the cell cycle, determined from the proteomic dataset
1479 described in Figure 1. **(C)** Cyclin D**, (D)** CDK4**, (E)** CDK6**, (F)** p27Kip1.

1480 **(G-H)** B cells were purified from the spleens of C57BL6/J mice and stimulated with
1481 LPS (20µg/ml) and IL-4 (10ng/ml) for 24 hours before fixing and staining for phospho-
1482 retinoblastoma (p-Rb). Gating strategy for p-Rb staining is shown in Figure S14B. **(G)**
1483 Representative histogram comparing p-Rb staining in naïve and LPS + IL-4 stimulated
1484 B cells. **(H)** Quantification shows three technical replicates from cells isolated from one
1485 mouse and is representative of three independent experiments.

1486 **(I)** Heat map showing the expression of proteins encoded by E2F target genes, derived
1487 from the proteomic data.

1488 **(J-M)** Graphs depicting changes in the estimated cellular concentration (nM) of
1489 proteins implicated in cell cycle progression, determined from the proteomic dataset
1490 described in Figure 1. **(J)** Cyclin A, **(K)** Cyclin B, **(L)** CDK2, **(M)** CDK1.

1491 p values were determined using an unpaired two-tailed Student's t-test for **(H)** or
1492 represent adjusted p values from the FDR calculations applied to the proteomic
1493 dataset **(D, E, F, L)**, where $p<0.01$ is indicated by **, $p<0.001$ by *** and $p<0.0001$ by
1494 ****.

1495

1496 **Figure 3. LPS + IL-4 stimulation promotes protein synthesis**

1497 **(A, B)** Graphs show changes in cellular concentration (nM) of the sum of proteins that
1498 make up the large **(A)** and small **(B)** ribosomal subunits, with heat maps showing the
1499 expression of the individual proteins making up the large **(C)** and small **(D)** subunits.

1500 **(E-G)** The proteomic dataset was mined for proteins involved in the biogenesis of the
1501 large and small ribosomal subunits based on the GO terms: GO:0000027,
1502 GO:0042273, GO:0000028, GO:0042274. **(E)** shows the sum of the proteins involved
1503 in the biogenesis of the large subunit and **(F)** shows the small subunit, with individual
1504 proteins represented on the volcano plot **(G)** Horizontal dashed lines on (G) indicate q
1505 < 0.05 while vertical dashed lines indicate $\log_2$ fold change more than one standard
1506 deviation away from the median.

1507 **(H-I)** Splenocytes from C57BL6/J mice were stimulated with LPS (20µg/ml) and IL-4
1508 (10ng/ml) for 24 hours before fixing and staining for the uptake of puromycin analog
1509 O-propargyl-puromycin (OPP) to measure protein synthesis. Gating strategy for OPP
1510 staining is shown in Figure S14C. **(H)** Representative histogram comparing OPP
1511 uptake between naïve and LPS + IL-4 stimulated B cells. **(I)** Quantification shows three
1512 technical replicates from cells isolated from one mouse. Statistical power was
1513 determined using an unpaired two-tailed Student's t-test, where $p<0.001$ is indicated
1514 by *** and $p<0.0001$ by ****.

1515

1516 **Figure 4. Amino acid transporter SLC7A5 is required for key B cell functions**

1517 **(A)** Heat map showing the expression of genes encoding for proteins involved in
1518 plasma membrane amino acid transport determined from the proteomic dataset
1519 described in Figure 1.

1520 **(B, C)** Graphs depicting changes in cellular concentration (nM) of **(B)** SLC7A5 and **(C)**
1521 SLC3A2 derived from the proteomic data. A*p(adj)* of <0.0001, based on the proteomic
1522 FDR calculations, is indicated by ****.

1523 **(D-E)** Lymph node cells from C57BL6/J mice were stimulated with LPS (20µg/ml) and
1524 IL-4 (10ng/ml) for 24 hours before staining for CD98. **(D)** Representative FACS plot
1525 comparing CD98 expression. **(E)** Quantification shows three technical replicates from
1526 cells isolated from one mouse and is representative of two independent experiments.

1527 Statistical power was determined using one-way ANOVA followed by multiple
1528 comparison testing via Dunnett's analysis. For comparison to naïve B cells, where
1529 $p<0.001$ is indicated by *** and $p<0.0001$ by ****.

1530 **(F-I)** B cells were purified from the spleens of wild type (WT) and *Slc7a5* $^{fl/fl}$/Vav-iCre^{+ve}
1531 mice and stained with CTV before stimulation with LPS (20µg/ml) and IL-4 (10ng/ml)
1532 for 72 hours. **(F)** Percentage of live B cells (7AAD-ve) in WT and *Slc7a5*$^{fl/fl}$/Vav-
1533 iCre^{+ve}mice. **(G)** Histogram representing CTV staining of WT and *Slc7a5*$^{fl/fl}$/Vav-iCre^{+ve}
1534 B cells. **(H)** Live B cell number of WT and *Slc7a5*$^{fl/fl}$/Vav-iCre^{+ve}mice. **(I)** Percentage of
1535 B cells that are IgG1+ve in WT and *Slc7a5*$^{fl/fl}$/Vav-iCre^{+ve}mice. Data shows the results
1536 of four biological replicates per genotype. $p<0.0001$ is indicated by **** (unpaired
1537 two-tailed Student's t-test).

1538 **(J-K)** B cells were purified from the spleens of WT and *Slc7a5*$^{fl/fl}$/Vav-iCre^{+ve}mice and
1539 stimulated with LPS (20µg/ml) +/- IL-4 (10ng/ml) for 24 hours before fixing and staining
1540 for the uptake of kynurenine to measure amino acid uptake. Gating strategy for
1541 kynurenine uptake in Figure S14D. **(J)** Quantification of kynurenine MFI between B
1542 cells from WT and SLC7A5 KO mice with (+) or without (-) LPS + IL-4, kynurenine or
1543 aminobicyclo-(2,2,1)-heptane-2-carboxylic acid (BCH). **(K)** Quantification of
1544 kynurenine MFI between B cells from WT and *Slc7a5*$^{fl/fl}$/Vav-iCre^{+ve}mice with (+) or
1545 without (-) LPS, kynurenine or BCH. Data shows the results of four biological replicates
1546 per genotype. Statistical power was determined for using two-way ANOVA followed by
1547 multiple comparison testing via Sidak's analysis, where $p<0.0001$ is indicated by ****
1548 for comparisons between genotypes.

1549 **Figure 5. LPS + IL-4 stimulation upregulates cholesterol metabolism in B cells**

1550 **(A-E)** Analysis of the genes involved in cholesterol metabolism in the proteomic
1551 dataset. **(A)** Heat map of all the enzymes involved in cholesterol biosynthesis. Cellular
1552 concentration (nM) of **(B)** HMGCR, **(C)** SQLE, **(D)** LDLR, and **(E)**. A *p(adj)* of <0.01 is
1553 indicated by **.

1554 **(F)** Splenocytes from C57BL6/J mice were plated in cholesterol-free (CF) media and
1555 stimulated with LPS (20µg/ml) and IL-4 (10ng/ml). The cells were fixed at the stated
1556 time points and stained with filipin. The gating strategy for filipin staining in Figure
1557 S15A. **(F)** Filipin timecourse. Data shows three technical replicates from cells isolated
1558 from one mouse. Statistical power was determined by one-way ANOVA followed by

1559 multiple comparison testing via Dunnett's analysis. For comparisons to naïve B cells,
1560 $p<0.05$ is indicated by * and $p<0.0001$ by ****.

1561 **(G-H)** Splenocytes from C57BL6/J mice were plated in cholesterol-free media and pre-
1562 treated with DMSO as a vehicle control or varying concentrations of Fluvastatin or NB-
1563 598 for 45 minutes before stimulation with LPS (20µg/ml) and IL-4 (10ng/ml). The cells
1564 were fixed after 24 hours and stained with filipin before acquisition. **(G)** Filipin staining
1565 of Fluvastatin titration. **(H)** Filipin staining of NB-598 titration. Data shows three
1566 technical replicates from cells isolated from one mouse and is representative of two
1567 independent experiments, each with one biological replicate. Statistical power was
1568 determined using a one-way ANOVA followed by multiple comparison testing via
1569 Dunnett's analysis. For comparison to LPS + IL-4 stimulated B cells, $p<0.001$ is
1570 indicated by *** and $p<0.0001$ by ****.

1571 **(I)** Spleenocytes from C57BL6/J mice were plated in normal or cholesterol-free (CF)
1572 media and pre-treated with DMSO as a vehicle control, Fluvastatin (10µM) or NB-598
1573 (10µM) before stimulation with LPS + IL-4. The cells were fixed after 24 hours and
1574 stained with filipin before acquisition. Data shows the results of three biological
1575 replicates. Statistical power was determined using two-way ANOVA followed by
1576 multiple comparison testing via Tukey's analysis. For comparisons to the LPS + IL-4
1577 condition, $p<0.0001$ is indicated by ****.

1578

1579 **Figure 6. Blocking rate-limiting enzymes in the cholesterol biosynthesis**
1580 **pathway reduces B cell growth, survival and proliferation**

1581 **(A-D)** B cells were purified from the spleens of C57BL6/J mice and cultured in normal
1582 or cholesterol-free (CF) media. The cells were stained with CTV, then pre-treated with
1583 DMSO as a vehicle control or Fluvastatin (10µM) or NB-598 (10µM), where indicated,
1584 for 45 minutes prior to stimulation with LPS (20µg/ml) and IL-4 (10µg/ml) for 48 hours.
1585 Gating strategy for CTV staining is shown in Figure S15B. **(A)** shows representative
1586 CTV staining, **(B)** live B cell number, **(C)** percentage of live B cells (7AAD-ve) and **(D)**
1587 forward scatter. Data shows the results of three biological replicates.

1588 **(E-H)** Same as **(A-D)** but with pretreatment using FGTI-2734 (10µM). **(E)** shows
1589 representative CTV staining, **(F)** live B cell number, **(G)** percentage of live B cells

1590 (7AAD-ve) and **(H)** forward scatter of B cells. Data shows the results of three biological
1591 replicates.

1592 **(I-P)** Same as **(A-D)** but with pretreatment using FTI-277 or GGTI-298 (10μM-30μM).
1593 **(I)** shows representative CTV staining in normal media, **(J)** live B cell number, **(K)**
1594 percentage of live B cells (7AAD-ve) and **(L)** forward scatter of B cells. **(M)** shows
1595 representative CTV staining in CF media, **(N)** live B cell number, **(O)** percentage of
1596 live B cells (7AAD-ve) and **(P)** forward scatter of B cells. Data shows the results of
1597 three biological replicates.

1598 **(B-D) (F-H)** Statistical power was determined using two-way ANOVA followed by
1599 multiple comparison testing via Tukey's analysis. For comparisons to the LPS + IL-4
1600 condition, $p<0.01$ is indicated by **, $p<0.001$ by *** and $p<0.0001$ by ****. ns indicated
1601 by $p>0.05$. **(J-L) (N-P)** Statistical power was determined using one-way ANOVA
1602 followed by multiple comparison testing via Dunnett's analysis. For comparisons to the
1603 LPS + IL-4 condition, $p<0.01$ is indicated by **, $p<0.001$ by *** and $p<0.0001$ by ****.
1604 ns indicated by $p>0.05$. For all panels, cells in the absence of LPS + IL-4 were naïve
1605 B cells analysed on the day of isolation.

1606

1607 **Figure 7. Mevalonate supplementation rescues the effect of Fluvastatin**
1608 **treatment in B cells**

1609 **(A-B)** Splenocytes from C57BL6/J mice were plated in normal or cholesterol-free (CF)
1610 media and pre-treated with HEPES as a vehicle control or mevalonate (2mM) for 1
1611 hour prior to treatment with DMSO or Fluvastatin (10μM), where indicated, for 45
1612 minutes before stimulation with LPS (20μg/ml) and IL-4 (10ng/ml). The cells were fixed
1613 after 24 hours or 48 hours of LPS + IL-4 stimulation and stained with filipin. **(A)** Filipin
1614 staining comparing B cells +/- Fluvastatin or mevalonate after 24 or 48 hours of LPS
1615 + IL-4 stimulation in normal media. **(B)** Filipin staining comparing B cells +/- Fluvastatin
1616 or mevalonate after 24 or 48 hours of LPS + IL-4 stimulation in CF media. Data shows
1617 the results of three biological replicates.

1618 **(C-F)** B cells were purified from the spleens of C57BL6/J mice and cultured in normal
1619 or cholesterol-free media. The cells were stained with CTV, then pre-treated with
1620 HEPES as a vehicle control or mevalonate (2mM) for 1 hour. The cells were treated
1621 with DMSO or Fluvastatin (10μM), where indicated, for 45 minutes prior to stimulation

1622 with LPS (20μg/ml) and IL-4 (10μg/ml) for 48 hours. **(C)** Shows percentage of live B
1623 cells (7AAD-ve), **(D)** forward scatter of B cells, **(E)** representative CTV staining and **(F)**
1624 live B cell number. Data shows the results of three biological replicates. Where shown,
1625 statistical power was determined using two-way ANOVA followed by multiple
1626 comparison testing via Sidak's analysis. For comparison to Fluvastatin treated B cells,
1627 $p<0.05$ is indicated by *, $p<0.01$ by **, $p<0.001$ by ***, $p<0.0001$ by ****. ns by >0.05.
1628 For all panels, cells in the absence of LPS + IL-4 were naïve B cells analysed on the
1629 day of isolation.

1630

1631 **Figure 8. GGPP supplementation rescues the effect of Fluvastatin treatment in**
1632 **B cells**

1633 **(A-H)** B cells were purified from the spleens of C57BL6/J mice and cultured in normal
1634 or cholesterol-free media. The cells were stained with CTV, pre-treated with
1635 methanol:ammonium hydroxide solution (CH3OH:NH4OH) as a vehicle control or
1636 geranylgeranyl pyrophosphate (GGPP) (10μM) for 1 hour before treatment with
1637 Fluvastatin (10μM), where indicated. The cells were stimulated with LPS (20μg/ml)
1638 and IL-4 (10μg/ml) and cultured for 48 hours. **(A)** shows representative CTV staining
1639 for B cells cultured in normal media, **(B)** live B cell number, **(C)** percentage of live B
1640 cells and **(D)** forward scatter of B cells. **(E)** shows representative CTV staining for B
1641 cells cultured in CF media, **(F)** live B cell number, **(G)** percentage of live B cells and
1642 **(H)** forward scatter of B cells.

1643

1644 Data shows the results of three biological replicates. Statistical power was determined
1645 using one-way ANOVA followed by multiple comparison testing via Dunnett's analysis.
1646 For comparison to Fluvastatin treated B cells, $p<0.001$ is indicated by *** and $p<0.0001$
1647 by ****. ns indicated $p>0.05$. For **(B)** and **(F)** this data was log-transformed then
1648 statistically analysed due to unequal variance.

1649

1650 **(I-J)** Splenocytes were plated in normal or cholesterol-free media and pre-treated with
1651 methanol:ammonium hydroxide solution (CH3OH:NH4OH) as a vehicle control or
1652 geranylgeranyl pyrophosphate (GGPP) (10μM), where indicated, for 1 hour before
1653 treatment with DMSO or Fluvastatin (10μM). The cells were then stimulated with LPS
1654 (20μg/ml) and IL-4 (10ng/ml). The cells were fixed after 24 hours and stained with

1655 filipin before acquisition. **(I)** Filipin staining comparing B cells +/- Fluvastatin or GGPP
1656 after 24 or 48 hours of LPS + IL-4 stimulation in normal media. **(J)** Filipin staining
1657 comparing B cells +/- Fluvastatin or GGPP after 24 or 48 hours of LPS + IL-4
1658 stimulation in CF media.

1659 Data shows the results of three biological replicates. Statistical power was determined
1660 using two-way ANOVA followed by multiple comparison testing via Sidak's analysis.
1661 For comparison to Fluvastatin treated B cells, $p<0.01$ is indicated by **, $p<0.001$ by
1662 *** and $p<0.0001$ by ****. ns indicated $p>0.05$. For all panels, cells in the absence of
1663 LPS + IL-4 were naïve B cells analysed on the day of isolation.

1664

1665 **Figure 9. MAPK and mTOR signalling regulate B cell proliferation and**
1666 **cholesterol levels**

1667 **(A-E)** B cells were purified from the spleens of C57BL6/J mice and stained with CTV,
1668 then pre-treated with DMSO as a vehicle control, PD18352 (2μM), VX745 (1μM) or
1669 Rapamycin (20nM), where indicated, for 45 minutes prior to stimulation with LPS
1670 (20μg/ml) and IL-4 (10μg/ml) for 48 hours. **(A)** shows representative CTV staining, **(B)**
1671 percentage of B cells per generation quantified from **(A)**, **(C)** live B cell number **(D)**
1672 percentage of live B cells (7AAD-ve) and **(E)** forward scatter. Data shows three
1673 technical replicates from cells isolated from one mouse and is representative of three
1674 independent experiments. Statistical power for **(B)** was determined using two-way
1675 ANOVA followed by multiple comparison testing via Sidak's analysis. For comparison
1676 to LPS + IL-4 stimulated B cells, $p<0.0001$ by **** and ns by >0.05.

1677 **(F)** Splenocytes from C57BL6/J mice were pre-treated with DMSO as a vehicle control,
1678 PD18352 (2μM), VX745 (1μM) or Rapamycin (20nM), where indicated, for 45 minutes
1679 prior to stimulation with LPS (20μg/ml) and IL-4 (10μg/ml). The cells were fixed after
1680 24 hours and stained with filipin before acquisition. **(F)** Filipin staining after inhibitor
1681 treatment.

1682 Statistical power was determined by one-way ANOVA followed by multiple comparison
1683 testing via Dunnett's analysis, where $p<0.05$ is indicated by *, $p<0.01$ by **, $p<0.001$
1684 by ***, $p<0.0001$ by **** and ns by >0.05. For all panels, cells in the absence of LPS +
1685 IL-4 were naïve B cells analysed on the day of isolation.

1686

1687 **Figure 10. Cholesterol is required for the growth and proliferation of B cells by**
1688 **multiple stimuli**

1689 **(A)** Splenocytes from C57BL6/J mice were plated in normal or CF media, before
1690 stimulation with LPS (20µg/ml), IL-4 (10µg/ml) or a combination of LPS and IL-4.
1691 stimuli. The cells were fixed after 24 hours and stained with filipin. **(A)** Filipin staining
1692 comparing cholesterol content between different stimuli. Data shows the results of
1693 three biological replicates. Statistical power was determined using two-way ANOVA
1694 followed by multiple comparison testing via Tukey's analysis. For comparisons to naïve
1695 B cells, $p<0.0001$ is indicated by ****.

1696 **(B)** Splenocytes from C57BL6/J mice were plated in normal media before stimulation
1697 with LPS (20µg/ml), Resiquimod (1µg/ml), ODN 1826 (1µg/ml), Anti-IgM (10µg/ml), or
1698 CD40L (500ng/ml). The cells were fixed after 24 hours and stained with filipin. **(B)**
1699 Filipin staining comparing cholesterol content between different stimuli. Data shows
1700 the results of three biological replicates. Statistical power was determined using one-
1701 way ANOVA followed by multiple comparison testing via Dunnett's analysis. For
1702 comparisons to naïve B cells, $p<0.0001$ is indicated by ****.

1703 **(C-E)** B cells were purified from the spleens of C57BL6/J mice and cultured in normal
1704 media. The cells were stained with CTV, then pre-treated with DMSO as a vehicle
1705 control or Fluvastatin (10µM) for 45 minutes before stimulation with LPS (20µg/ml),
1706 Resiquimod (1µg/ml), ODN 1826 (1µg/ml), Anti-IgM (10µg/ml), or CD40L (500ng/ml)
1707 as indicated for 72 hours. **(C)** shows the percentage of live B cells (7AAD-ve), **(D)**
1708 representative histogram for CTV staining and **(E)** live B cell number. Data shows the
1709 results of three biological replicates. Statistical power was determined using two-way
1710 ANOVA followed by multiple comparison testing via Tukey's analysis, where $p<0.0001$
1711 is indicated by ****. For **(E),** this data was log-transformed and then statistically
1712 analysed due to unequal variance. Statistical power was determined using two-way
1713 ANOVA followed by multiple comparison testing via Sidak's analysis, where $p<0.0001$
1714 is indicated by ****.

Figure 1

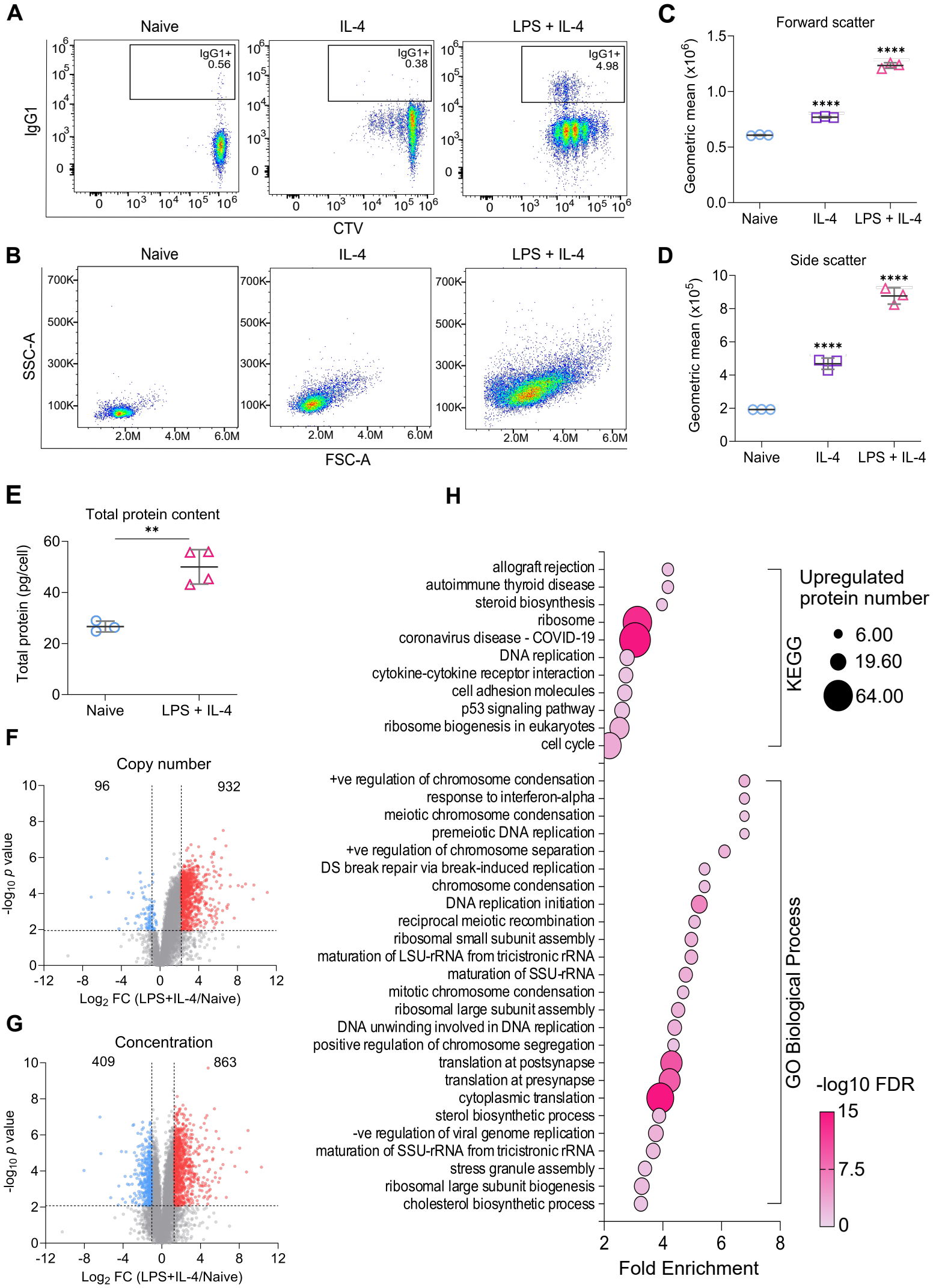
A
Naive
IL-4
LPS + IL-4
IgG1+ 0.56
IgG1+ 0.38
IgG1+ 4.98
IgG1
CTV
B
SSC-A
FSC-A
C
Forward scatter
Geometric mean (x10^6)
****
D
Side scatter
Geometric mean (x10^5)
E
Total protein content
**
Total protein (pg/cell)
F
Copy number
96
932
-log10 p value
Log2 FC (LPS+IL-4/Naive)
G
Concentration
409
863
H
allograft rejection
autoimmune thyroid disease
steroid biosynthesis
ribosome
coronavirus disease - COVID-19
DNA replication
cytokine-cytokine receptor interaction
cell adhesion molecules
p53 signaling pathway
ribosome biogenesis in eukaryotes
cell cycle
KEGG
Upregulated protein number
6.00
19.60
64.00
+ve regulation of chromosome condensation
response to interferon-alpha
meiotic chromosome condensation
premeiotic DNA replication
+ve regulation of chromosome separation
DS break repair via break-induced replication
chromosome condensation
DNA replication initiation
reciprocal meiotic recombination
ribosomal small subunit assembly
maturation of LSU-rRNA from tricistronic rRNA
maturation of SSU-rRNA
mitotic chromosome condensation
ribosomal large subunit assembly
DNA unwinding involved in DNA replication
positive regulation of chromosome segregation
translation at postsynapse
translation at presynapse
cytoplasmic translation
sterol biosynthetic process
-ve regulation of viral genome replication
maturation of SSU-rRNA from tricistronic rRNA
stress granule assembly
ribosomal large subunit biogenesis
cholesterol biosynthetic process
GO Biological Process
-log10 FDR
Fold Enrichment

Figure 2

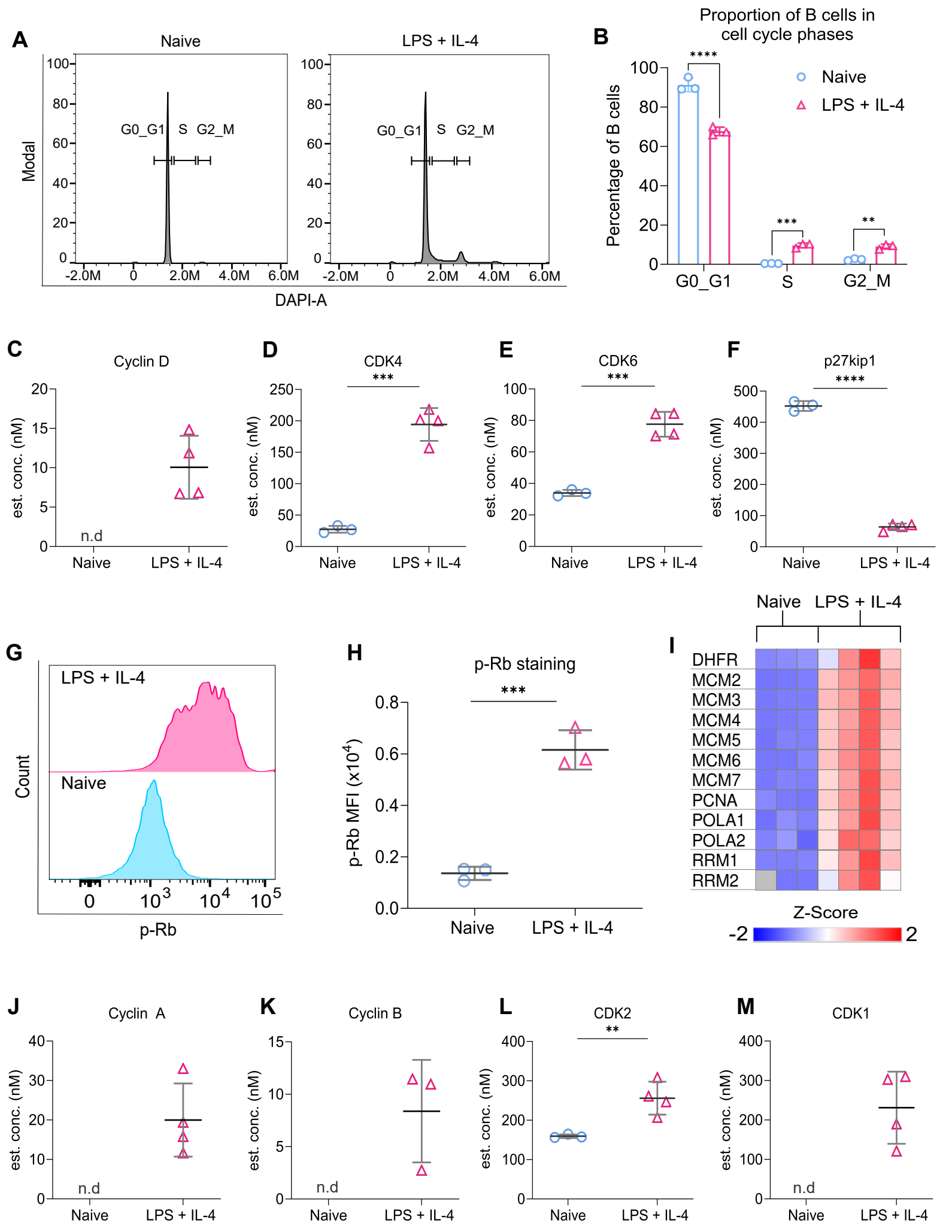
A
Naive
LPS + IL-4
Modal
G0_G1
S
G2_M
DAPI-A
B
Proportion of B cells in cell cycle phases
Percentage of B cells
Naive
LPS + IL-4
G0_G1
S
G2_M
C
Cyclin D
est. conc. (nM)
n.d
D
CDK4
E
CDK6
F
p27kip1
G
LPS + IL-4
Naive
Count
p-Rb
H
p-Rb staining
p-Rb MFI (x10^4)
I
DHFR
MCM2
MCM3
MCM4
MCM5
MCM6
MCM7
PCNA
POLA1
POLA2
RRM1
RRM2
Z-Score
J
Cyclin A
K
Cyclin B
L
CDK2
M
CDK1

Figure 3

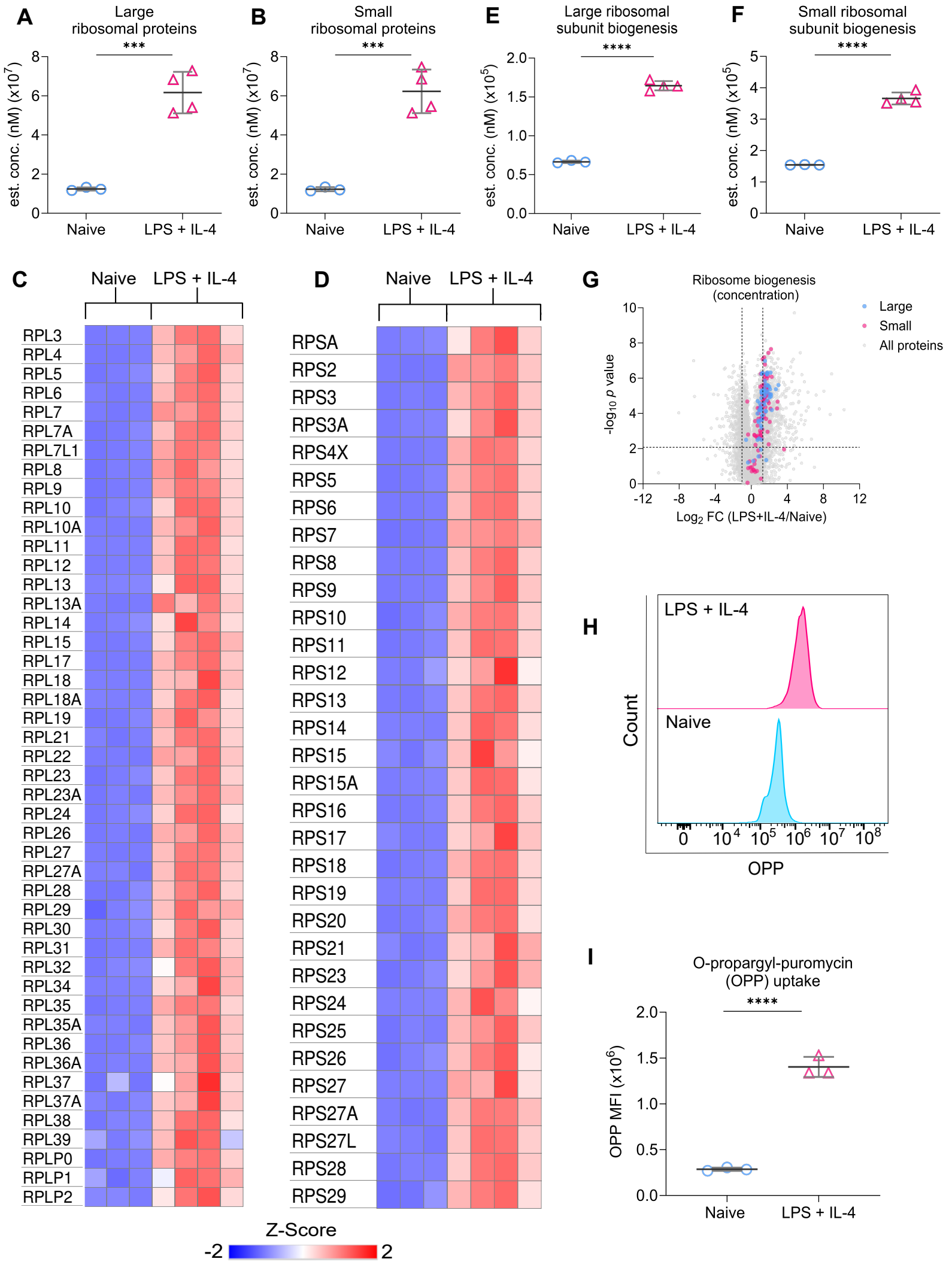
A
Large ribosomal proteins
***
est. conc. (nM) (x10^7)
Naive
LPS + IL-4
B
Small ribosomal proteins
***
est. conc. (nM) (x10^7)
E
Large ribosomal subunit biogenesis
****
est. conc. (nM) (x10^5)
F
Small ribosomal subunit biogenesis
****
est. conc. (nM) (x10^5)
C
Naive
LPS + IL-4
RPL3
RPL4
RPL5
RPL6
RPL7
RPL7A
RPL7L1
RPL8
RPL9
RPL10
RPL10A
RPL11
RPL12
RPL13
RPL13A
RPL14
RPL15
RPL17
RPL18
RPL18A
RPL19
RPL21
RPL22
RPL23
RPL23A
RPL24
RPL26
RPL27
RPL27A
RPL28
RPL29
RPL30
RPL31
RPL32
RPL34
RPL35
RPL35A
RPL36
RPL36A
RPL37
RPL37A
RPL38
RPL39
RPLP0
RPLP1
RPLP2
D
Naive
LPS + IL-4
RPSA
RPS2
RPS3
RPS3A
RPS4X
RPS5
RPS6
RPS7
RPS8
RPS9
RPS10
RPS11
RPS12
RPS13
RPS14
RPS15
RPS15A
RPS16
RPS17
RPS18
RPS19
RPS20
RPS21
RPS23
RPS24
RPS25
RPS26
RPS27
RPS27A
RPS27L
RPS28
RPS29
Z-Score
-2
2
G
Ribosome biogenesis (concentration)
Large
Small
All proteins
-log10 p value
Log2 FC (LPS+IL-4/Naive)
H
LPS + IL-4
Naive
Count
OPP
I
O-propargyl-puromycin (OPP) uptake
****
OPP MFI (x10^6)
Naive
LPS + IL-4

Figure 4

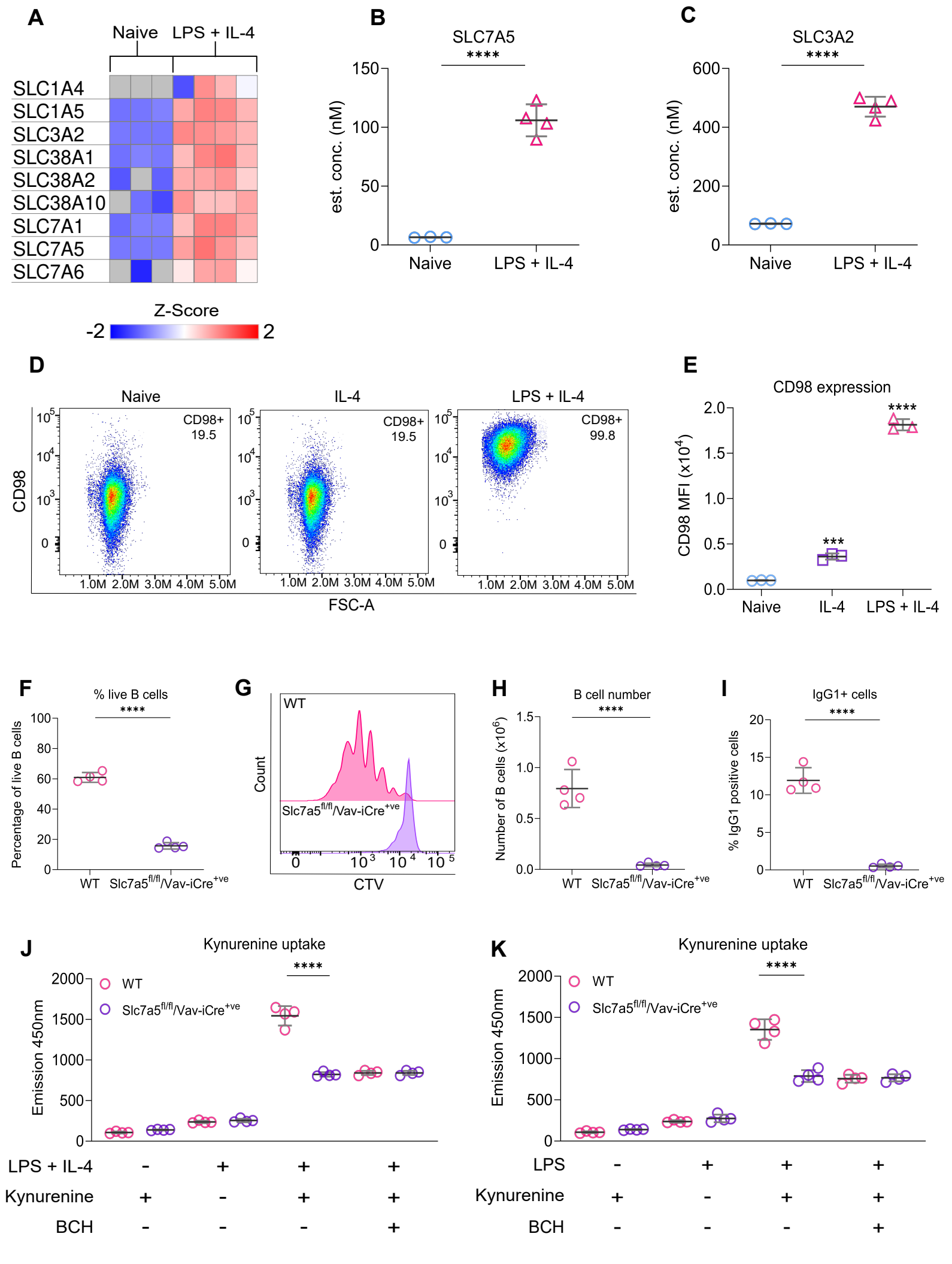
A
Naive
LPS + IL-4
SLC1A4
SLC1A5
SLC3A2
SLC38A1
SLC38A2
SLC38A10
SLC7A1
SLC7A5
SLC7A6
Z-Score
-2
2
B
SLC7A5
****
est. conc. (nM)
150
100
50
0
Naive
LPS + IL-4
C
SLC3A2
****
est. conc. (nM)
600
400
200
0
Naive
LPS + IL-4
D
Naive
IL-4
LPS + IL-4
CD98+
19.5
CD98+
19.5
CD98+
99.8
CD98
FSC-A
1.0M 2.0M 3.0M 4.0M 5.0M
E
CD98 expression
****
***
CD98 MFI (x10^4)
2.0
1.5
1.0
0.5
0.0
Naive
IL-4
LPS + IL-4
F
% live B cells
****
Percentage of live B cells
100
80
60
40
20
0
WT
Slc7a5fl/fl/Vav-iCre+ve
G
WT
Slc7a5fl/fl/Vav-iCre+ve
Count
CTV
H
B cell number
****
Number of B cells (x10^6)
1.5
1.0
0.5
0.0
WT
Slc7a5fl/fl/Vav-iCre+ve
I
IgG1+ cells
****
% IgG1 positive cells
20
15
10
5
0
WT
Slc7a5fl/fl/Vav-iCre+ve
J
Kynurenine uptake
****
WT
Slc7a5fl/fl/Vav-iCre+ve
Emission 450nm
2000
1500
1000
500
0
LPS + IL-4 - + + +
Kynurenine + - + +
BCH - - - +
K
Kynurenine uptake
****
WT
Slc7a5fl/fl/Vav-iCre+ve
Emission 450nm
2000
1500
1000
500
0
LPS - + + +
Kynurenine + - + +
BCH - - - +

Figure 5

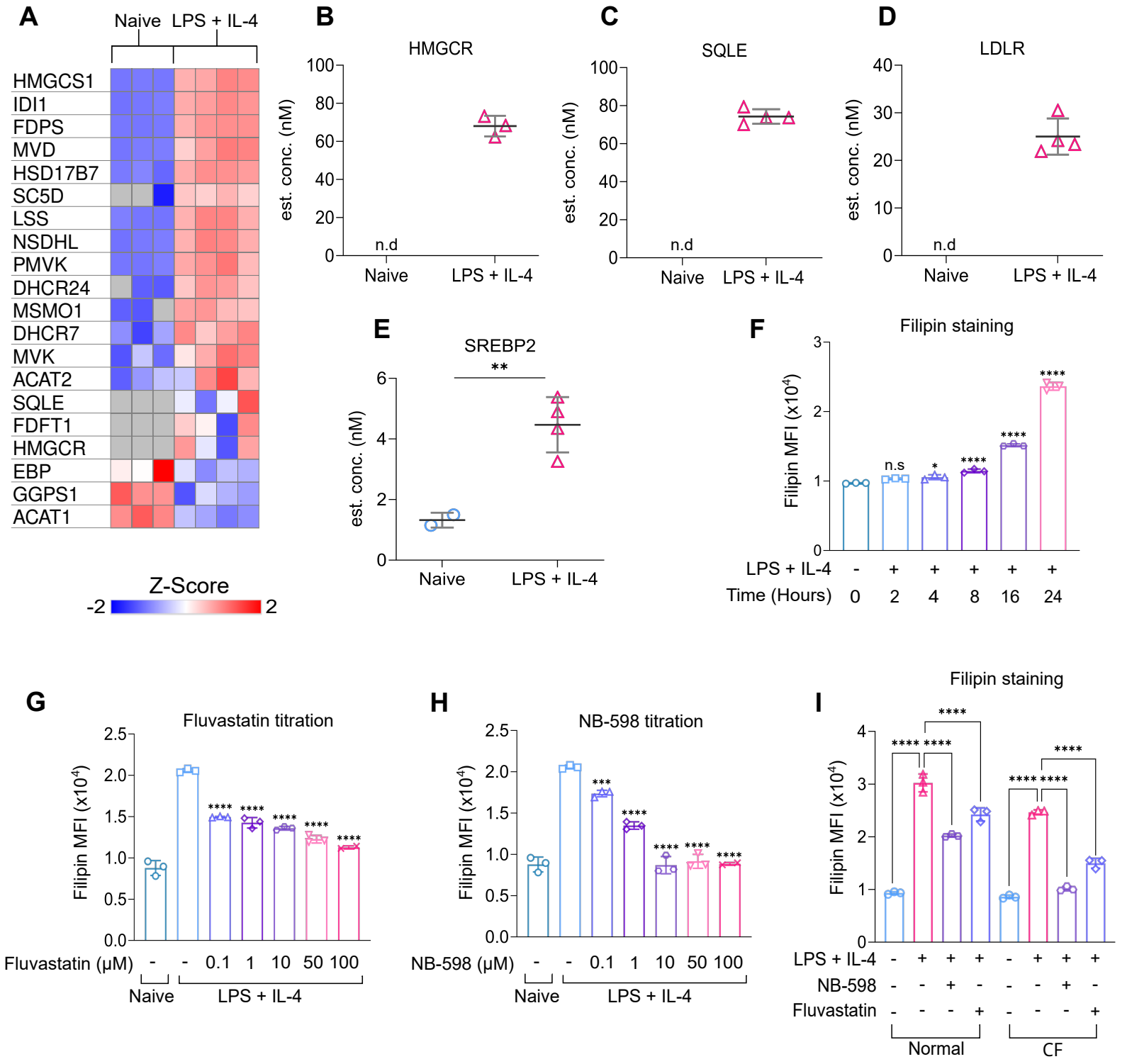
A
Naive
LPS + IL-4
HMGCS1
IDI1
FDPS
MVD
HSD17B7
SC5D
LSS
NSDHL
PMVK
DHCR24
MSMO1
DHCR7
MVK
ACAT2
SQLE
FDFT1
HMGCR
EBP
GGPS1
ACAT1
Z-Score
-2
2
B
HMGCR
est. conc. (nM)
n.d
Naive
LPS + IL-4
C
SQLE
est. conc. (nM)
n.d
Naive
LPS + IL-4
D
LDLR
est. conc. (nM)
n.d
Naive
LPS + IL-4
E
SREBP2
**
est. conc. (nM)
Naive
LPS + IL-4
F
Filipin staining
Filipin MFI (x10^4)
n.s
LPS + IL-4
Time (Hours)
0
2
4
8
16
24
G
Fluvastatin titration
Filipin MFI (x10^4)
Fluvastatin (μM)
0.1
1
10
50
100
Naive
LPS + IL-4
H
NB-598 titration
Filipin MFI (x10^4)
NB-598 (μM)
0.1
1
10
50
100
Naive
LPS + IL-4
I
Filipin staining
Filipin MFI (x10^4)
LPS + IL-4
NB-598
Fluvastatin
Normal
CF

Figure 6

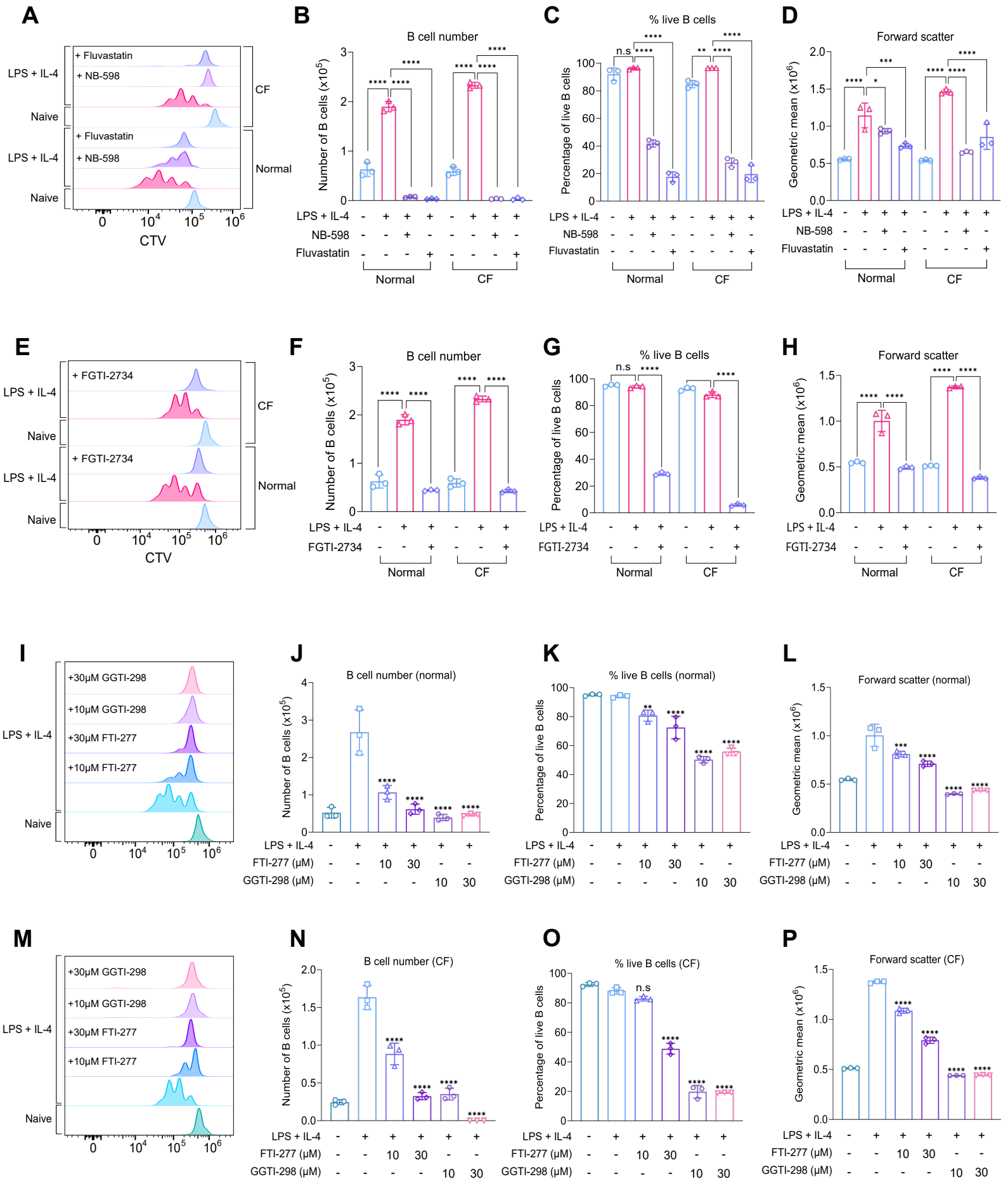
A
+ Fluvastatin
+ NB-598
LPS + IL-4
Naive
CF
Normal
CTV
B
B cell number
Number of B cells (x10^5)
C
% live B cells
Percentage of live B cells
D
Forward scatter
Geometric mean (x10^6)
LPS + IL-4
NB-598
Fluvastatin
Normal
CF
E
+ FGTI-2734
F
G
H
FGTI-2734
I
+30μM GGTI-298
+10μM GGTI-298
+30μM FTI-277
+10μM FTI-277
J
B cell number (normal)
K
% live B cells (normal)
L
Forward scatter (normal)
FTI-277 (μM)
GGTI-298 (μM)
M
N
B cell number (CF)
O
% live B cells (CF)
P
Forward scatter (CF)

Figure 7

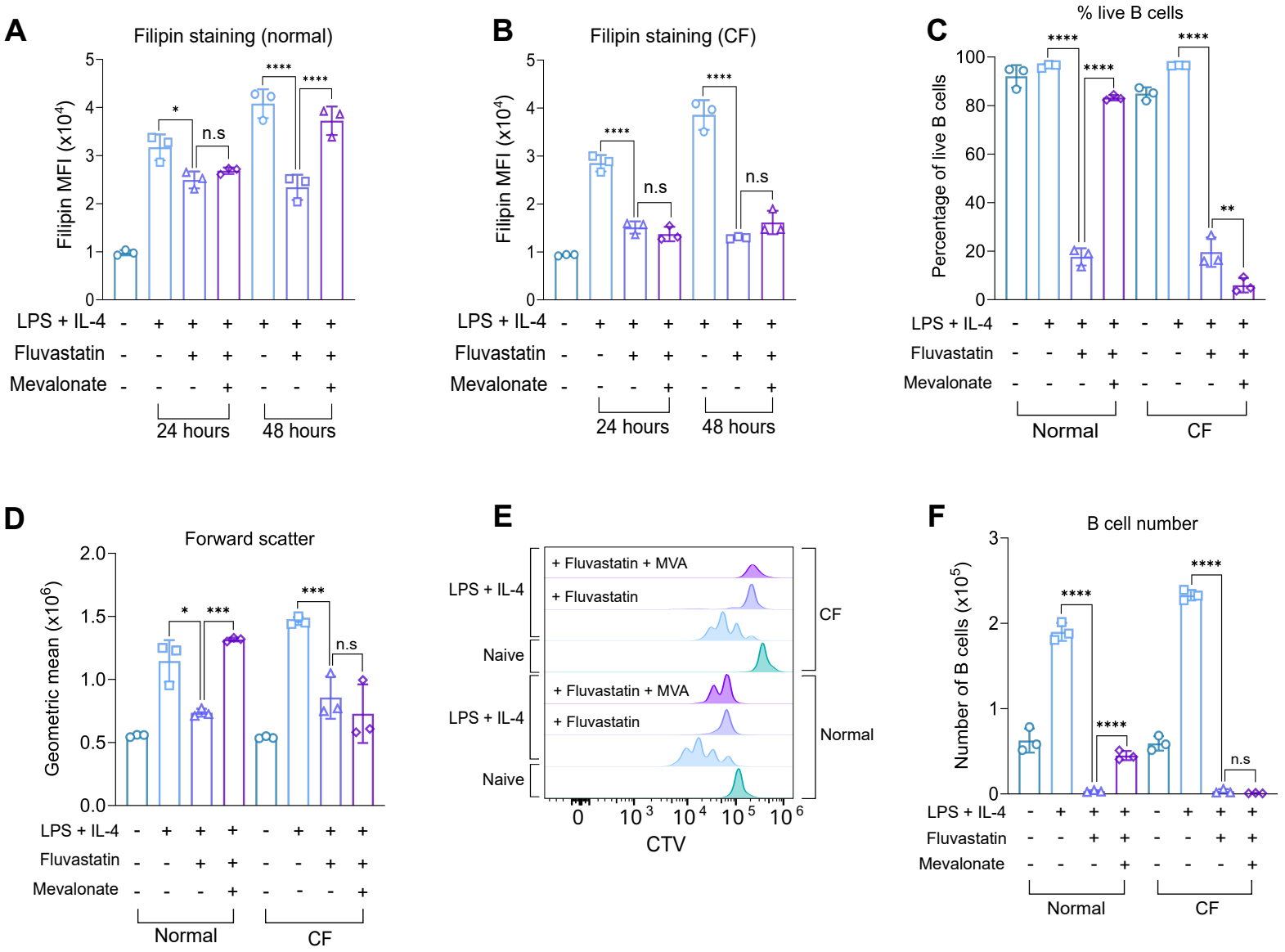
A
Filipin staining (normal)
Filipin MFI (x10^4)
LPS + IL-4
Fluvastatin
Mevalonate
24 hours
48 hours
B
Filipin staining (CF)
C
% live B cells
Percentage of live B cells
Normal
CF
D
Forward scatter
Geometric mean (x10^6)
E
+ Fluvastatin + MVA
+ Fluvastatin
Naive
CTV
F
B cell number
Number of B cells (x10^5)

Figure 8

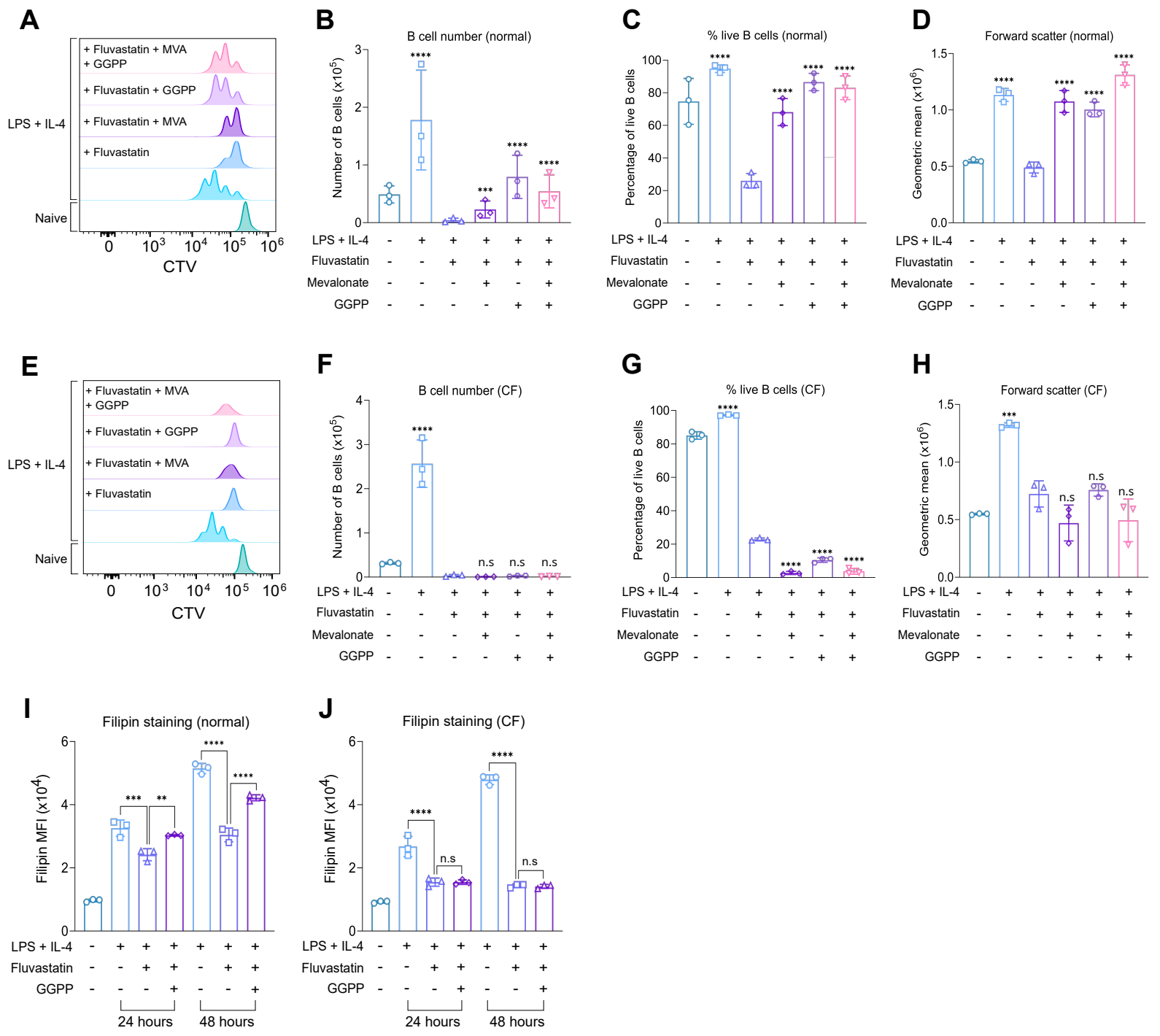
A
+ Fluvastatin + MVA + GGPP
+ Fluvastatin + GGPP
+ Fluvastatin + MVA
+ Fluvastatin
LPS + IL-4
Naive
CTV
B
B cell number (normal)
Number of B cells (x10^5)
C
% live B cells (normal)
Percentage of live B cells
D
Forward scatter (normal)
Geometric mean (x10^6)
LPS + IL-4
Fluvastatin
Mevalonate
GGPP
E
F
B cell number (CF)
G
% live B cells (CF)
H
Forward scatter (CF)
I
Filipin staining (normal)
Filipin MFI (x10^4)
J
Filipin staining (CF)
24 hours
48 hours

Figure 9

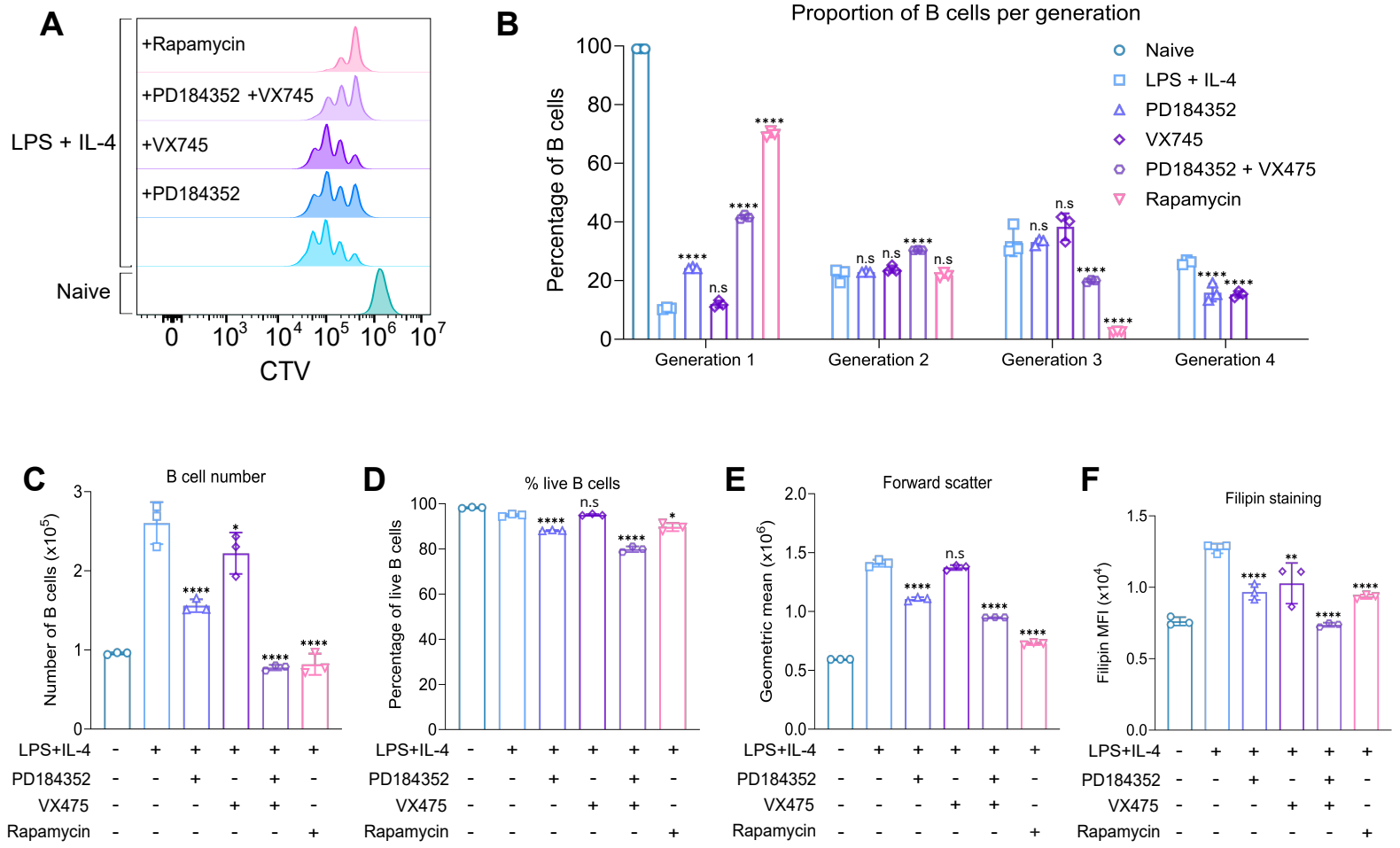
A
+Rapamycin
+PD184352 +VX745
+VX745
+PD184352
LPS + IL-4
Naive
0
10^3
10^4
10^5
10^6
10^7
CTV
B
Proportion of B cells per generation
Percentage of B cells
Naive
LPS + IL-4
PD184352
VX745
PD184352 + VX475
Rapamycin
Generation 1
Generation 2
Generation 3
Generation 4
C
B cell number
Number of B cells (x10^5)
D
% live B cells
Percentage of live B cells
E
Forward scatter
Geometric mean (x10^6)
F
Filipin staining
Filipin MFI (x10^4)
LPS+IL-4
PD184352
VX475
Rapamycin

Figure 10

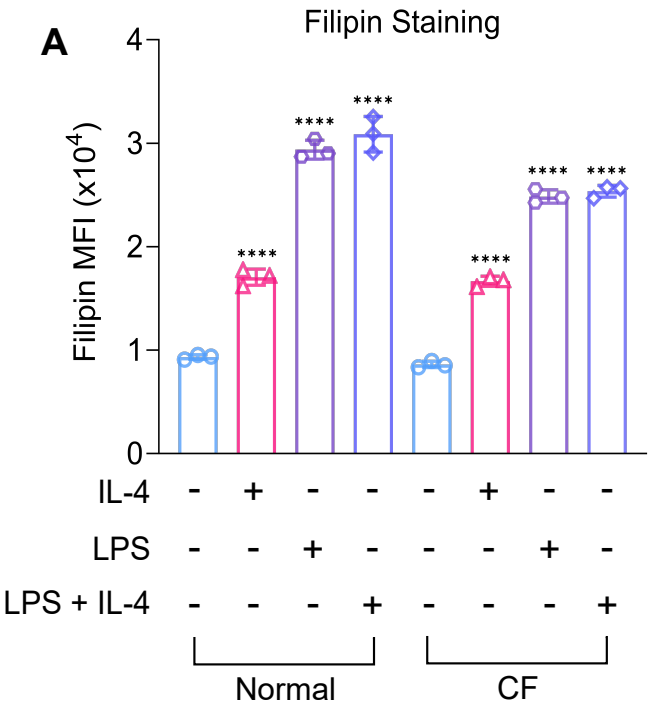
A
Filipin Staining
Filipin MFI (x10^4)
0
1
2
3
4
****
IL-4 - + - - - + - -
LPS - - + - - - + -
LPS + IL-4 - - - + - - - +
Normal
CF

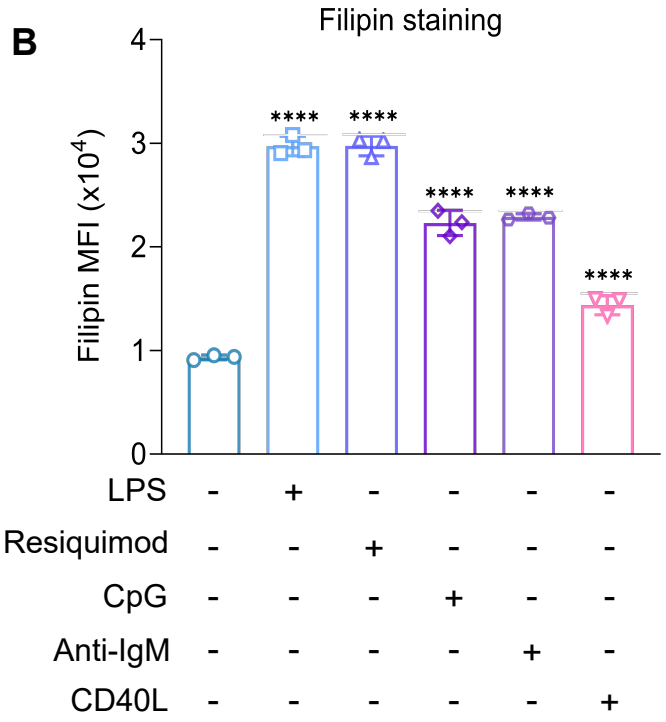
B
Filipin staining
Filipin MFI (x10^4)
0
1
2
3
4
****
LPS - + - - - -
Resiquimod - - + - - -
CpG - - - + - -
Anti-IgM - - - - + -
CD40L - - - - - +

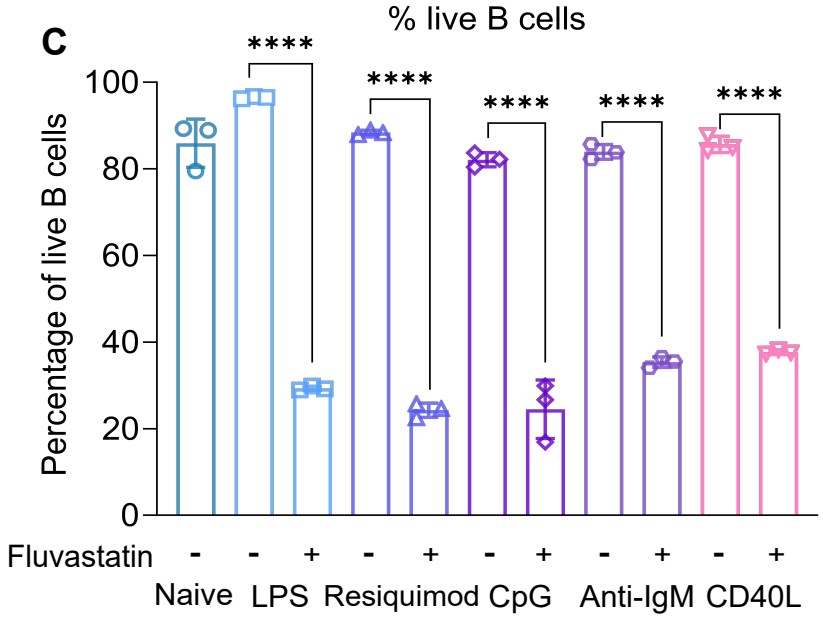
C
% live B cells
Percentage of live B cells
0
20
40
60
80
100
****
Fluvastatin - - + - + - + - + - +
Naive
LPS
Resiquimod
CpG
Anti-IgM
CD40L

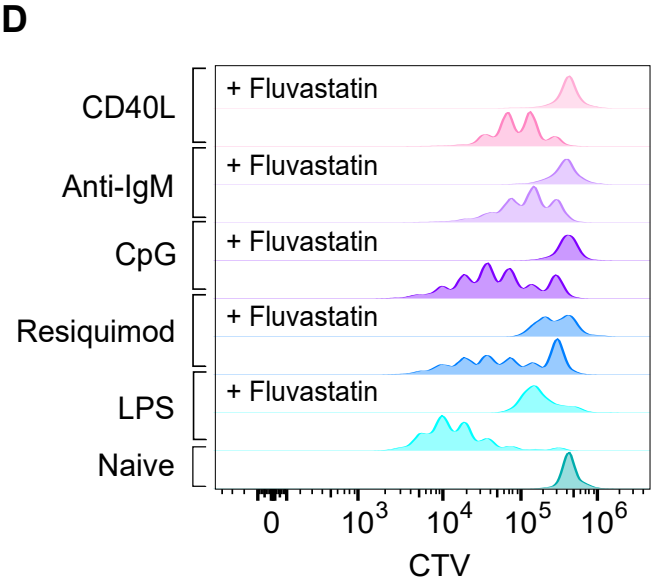
D
CD40L
Anti-IgM
CpG
Resiquimod
LPS
Naive
+ Fluvastatin
0
10^3
10^4
10^5
10^6
CTV

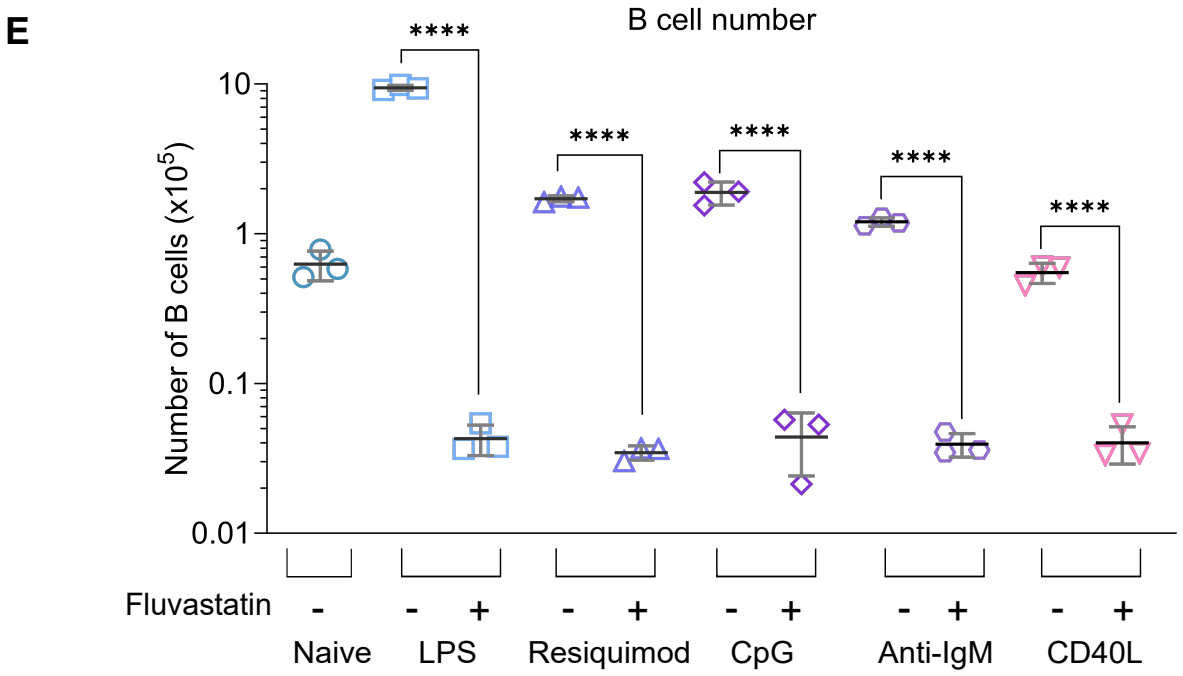
E
B cell number
Number of B cells (x10^5)
0.01
0.1
1
10
****
Fluvastatin - - + - + - + - + - +
Naive
LPS
Resiquimod
CpG
Anti-IgM
CD40L